

Comparison of Seismic and Structural Parameters of Settlements in the East Anatolian Fault Zone in Light of the 6 February Kahramanmaraş Earthquakes

Işık, Ercan; Hadzima-Nyarko, Marijana; Avcil, Fatih; Büyüksaraç, Aydın; Arkan, Enes; Alkan, Hamdi; Harirchian, Ehsan

Source / Izvornik: **Infrastructures**, 2024, 9

Journal article, Published version

Rad u časopisu, Objavljena verzija rada (izdavačev PDF)

<https://doi.org/10.3390/infrastructures9120219>

Permanent link / Trajna poveznica: <https://um.nsk.hr/um:nbn:hr:133:988630>

Rights / Prava: [Attribution-ShareAlike 4.0 International/Imenovanje-Dijeli pod istim uvjetima 4.0 međunarodna](#)

Download date / Datum preuzimanja: **2025-03-14**



GRAĐEVINSKI I ARHITEKTONSKI FAKULTET OSIJEK
Faculty of Civil Engineering and Architecture Osijek

Repository / Repozitorij:

[Repository GrAFOS - Repository of Faculty of Civil Engineering and Architecture Osijek](#)





Article

Comparison of Seismic and Structural Parameters of Settlements in the East Anatolian Fault Zone in Light of the 6 February Kahramanmaraş Earthquakes

Ercan Işık ¹, Marijana Hadzima-Nyarko ², Fatih Avcil ^{1,*}, Aydın Büyüksaraç ³, Enes Arkan ⁴, Hamdi Alkan ⁵ and Ehsan Harirchian ^{6,*}

¹ Department of Civil Engineering, Bitlis Eren University, 13100 Bitlis, Türkiye; eisik@beu.edu.tr

² Department of Civil Engineering, Josip Juraj Strossmayer University of Osijek, Vladimira Preloga 3, 31000 Osijek, Croatia; mhadzima@gfos.hr

³ Vocational School, Çanakkale 18 Mart University, 17400 Çanakkale, Türkiye; absarac@comu.edu.tr

⁴ Department of Architecture, Bitlis Eren University, 13100 Bitlis, Türkiye; earkan@beu.edu.tr

⁵ Department of Geophysics, Yüzüncü Yıl University, 65080 Van, Türkiye; hamdialkn@yyu.edu.tr

⁶ Institute of Structural Mechanics (ISM), Bauhaus-Universität Weimar, 99423 Weimar, Germany

* Correspondence: favcil@beu.edu.tr (F.A.); ehsan.harirchian@uni-weimar.de (E.H.)

Abstract: On 6 February 2023, two very large destructive earthquakes occurred in the East Anatolian Fault Zone (EAFZ), one of Türkiye's primary tectonic members. The fact that these earthquakes occurred on the same day and in the same region increased the extent of the destruction. Within the scope of this study, twenty different settlements affected by earthquakes and located directly on the EAFZ were taken into consideration. Significant destruction and structural failure at different levels were induced in reinforced concrete (RC) structures, the dominant urban building stock in these regions. To determine whether the earthquake hazard is adequately represented, the PGA values predicted in the last two earthquake hazard maps used in Türkiye for these settlements were compared with the measured PGAs from actual earthquakes. Subsequently, the damage to reinforced concrete structures in these settlements was evaluated within the scope of construction and earthquake engineering. In the final part of the study, static pushover analyses were performed on a selected example of a reinforced concrete building model, and target displacement values for different performance levels were determined separately for each earthquake. For the 20 different settlements considered, the displacements were also derived based on the values predicted in the last two earthquake hazard maps, and comparisons were made. While the target displacements were exceeded in some settlements, there was no exceedance in the other settlements. The realistic presentation of earthquake hazards will enable the mentioned displacements predicted for different performance levels of structures to be determined in a much more realistic manner. As a result, the performance grades predicted for the structures will be estimated more accurately.

Keywords: Kahramanmaraş; earthquake couple; reinforced concrete; PGA; target displacements



Citation: Işık, E.; Hadzima-Nyarko, M.; Avcil, F.; Büyüksaraç, A.; Arkan, E.; Alkan, H.; Harirchian, E. Comparison of Seismic and Structural Parameters of Settlements in the East Anatolian Fault Zone in Light of the 6 February Kahramanmaraş Earthquakes. *Infrastructures* **2024**, *9*, 219. <https://doi.org/10.3390/infrastructures9120219>

Academic Editor: Francesca Dezi

Received: 15 October 2024

Revised: 27 November 2024

Accepted: 30 November 2024

Published: 3 December 2024



Copyright: © 2024 by the authors. Licensee MDPI, Basel, Switzerland. This article is an open access article distributed under the terms and conditions of the Creative Commons Attribution (CC BY) license (<https://creativecommons.org/licenses/by/4.0/>).

1. Introduction

Total collapse, heavy damage, and different structural damage levels occurred in many different structural systems following the 6 February 2023 Kahramanmaraş earthquake, where the greatest loss of life and property occurred due to the instrumental period earthquake activity in Türkiye. The succession of the earthquakes and the large size of the region make these earthquakes unique to other earthquakes. Apart from the significant loss of life and property resulting from the earthquakes, the secondary economic losses have also been enormous. Both earthquakes occurred in the East Anatolian Fault Zone (EAFZ), one of the main tectonic elements of Türkiye. Investigations and evaluations of the structural damage following the earthquakes, which have caused major destruction to the

surrounding environment, provide a more realistic picture of the earthquake hazard and are a resource for developing earthquake-resistant building design principles.

It seems highly unlikely to be able to predict the magnitude, location, and timing of earthquakes with current technology. However, by using data obtained after an earthquake, the measures that can be taken before and during an earthquake can be based on a much more scientific and realistic foundation. In this context, the work carried out immediately after earthquakes is crucial both for realistically determining earthquake hazards and for identifying the shortcomings of earthquake-resistant building design standards [1–7]. Each study examining the earthquake hazard and structural damage after an earthquake is evaluated as a case study. These studies could be a source of support for both academia and decision-makers. In addition to studies examining the failure induced by earthquakes in various structural systems, both observationally and numerically, investigations into the risk of earthquakes have found their place in the literature. Some of these works are shown in Table 1.

Table 1. Some works about the characteristics of earthquakes and their effects on structures.

Country/Region	Year	Topic of the Study	Reference
Italy	2016	Damage causes and numerical analysis of typical Central Italian masonry residential buildings	Acito et al. [8]
Italy	2012	Evaluation of the earthquake damage in seven different masonry churches	Milani and Valente [9]
Chile	2010	Damage assessment of RC structures	Jünemann et al. [10]
Türkiye	2003	Assessment of the earthquake performance of RC buildings	Doğangün [11]
Italy	2012	Damage assessment of RC structures	Manfredi et al. [12]
Türkiye	2020	Impacts of the Sivrice earthquake on different structural systems	Nemutlu et al. [13]
Italy	2002	Effect of the Molise earthquake on RC buildings	Decanini et al. [14]
Croatia	2020	Post-earthquake evaluation and retrofitting of a historical building	Ademović et al. [15]
Taiwan	1999	Examination of the structural damage caused by the Chi-Chi earthquake in RC structures	Su [16]
New Zealand	2011	Evaluation of the damage caused by the Christchurch (Lyttleton) earthquake to RC structures	Kam et al. [17]
India	2001	Evaluation of the structural failures in RC structures after the Bhuj earthquake	Agarwal et al. [18]
Italy	2009	Investigation of damage to churches after an earthquake	Lagomarsino [19]
Malaysia	2015	Investigation of the damage in non-bearing elements of RC structures after the Ranau earthquake	Adiyanto et al. [20]
USA	1994	Ambient vibration experiments were performed for the 7-storey RC building damaged in the Northridge earthquake	Ivanović et al. [21]
Japan	1995	RC structures damaged by the Hyogo-ken Nanbu earthquake were taken into account	Nagato and Kawase [22]
Italy	2012	Investigation of the damage and failure mechanism of a castle	Valente and Milani [23]
Nepal	2015	Investigation of the heritage structures after an earthquake	Kumar et al. [24]
Greece	2021	Damage observed in masonry structures in an earthquake region	Sarhosis et al. [25]
China	2022	Rapid reporting of seismic damage after an earthquake	Qu et al. [26]
Philippines	2012	Evaluation of earthquake intensity and ShakeMap	Naik et al. [27]
Albania	2019	Seismic performance of modern RC buildings	Leti and Bilgin [28]
China	2022	Seismic behavior of multi-storey structures	Dong et al. [29]
New Zeland	2011	Investigation of structural and geotechnical damage	Tasiopoulou et al. [30]

In addition to these, some studies that have revealed the effects of the 6 February 2023 Kahramanmaraş earthquakes in the earthquake region, which is the subject of this study, are shown in Table 2.

Table 2. Some studies about the effects of the 6th of February Kahramanmaraş earthquakes.

Topic of the Study	Reference
Investigates the distribution of ground motion and its correlation with observed damage in southeastern Türkiye, highlighting how local soil conditions, valley effects, and the region’s tectonic structure contributed to significant amplification of seismic waves, particularly in areas like Antakya, Hassa, Kahramanmaraş, and Göksun.	Karray et al. [31]
Developed and tested an equation based on the MMI–PGA relationship to calculate earthquake intensity, refining intensity distribution maps for the 6 February 2023 earthquakes in southern Türkiye, and demonstrating that selected equations provided more sensitive, reliable, and objective results for assessing seismic impact.	Büyüksaraç et al. [32]
Examines the geotechnical and structural damage caused by the 6 February 2023 earthquakes in the Pazarçık and Elbistan districts of Kahramanmaraş, highlighting the critical role of soil–structure interactions and the lack of engineering in rural masonry buildings.	Akar et al. [33]
Damage in RC structures in the city center of Adıyaman was examined and structural analyses were carried out for a sample RC structural model.	Işık et al. [34]
Evaluate the effectiveness of one-dimensional nonlinear and equivalent linear site response analyses for assessing site effects during the 6 February 2023 Türkiye earthquakes.	İlhan et al. [35]
Damage in RC structures in the earthquake zone was evaluated based on deficiencies in earthquake regulations.	Öztürk et al. [36]
Analyzes the damage to reinforced concrete and steel buildings in Hatay following the 6 February 2023 earthquakes, identifying key issues such as construction defects, design errors, and structural failures, while offering recommendations based on seismic behavior studies and Turkish Building Earthquake Code guidelines.	Altunsu et al. [37]
Examines the 6 February 2023 earthquakes in Türkiye, highlighting the complex fault interactions, transtensional stress regime, and significant surface ruptures caused by the events, which resulted in over 100,000 building collapses and more than 50,000 fatalities.	Över et al. [38]
Analyzes the interconnection of the 6 February 2023 earthquakes in Türkiye using Coulomb stress analysis, showing how stress transfer between mainshocks and aftershocks contributed to widespread seismic activity and significant damage across multiple regions.	Alkan et al. [39]
Details a 10-day field reconnaissance by the International Consortium on Geo-disaster Reduction, focusing on seismic damage and ground failures caused by the 6 February 2023 earthquakes in southern Türkiye and northern Syria, with an emphasis on fault ruptures, liquefaction, and landslides.	Yan et al. [40]
Damage assessment of masonry and RC minarets in the earthquake zone and structural analyses for two minarets were selected as examples.	Atmaca et al. [41]
Evaluates the vulnerability of precast industrial buildings in Türkiye following the 6 February 2023 earthquakes, highlighting structural weaknesses, manufacturing defects, and the importance of code compliance, while recommending improvements to enhance seismic performance and prevent future damage.	Arslan et al. [42]
Examines seismically induced soil liquefaction during the 2023 Kahramanmaraş earthquakes in Türkiye, documenting surface manifestations, analyzing soil samples, and highlighting the unexpected liquefaction of clayey soils, suggesting a cautious approach to assessing the susceptibility of silty–clayey mixtures.	Cetin et al. [43]
Using the well-known ground motion prediction equations that are the foundation of Türkiye’s earthquake hazard map, the seismic properties of the recorded earthquake data are compared.	Öser et al. [44]
Presents findings from a field investigation of reinforced concrete structures damaged in the 6 February 2023 Kahramanmaraş earthquakes, analyzing structural and non-structural failures and offering recommendations for mitigating future earthquake-induced damage.	Sezgin et al. [45]

Table 2. Cont.

Topic of the Study	Reference
Analyzes the devastating effects of the 6 February 2023 earthquakes in Türkiye, highlighting the performance of buildings in relation to construction year, seismic code compliance, and the surprising vulnerability of newer structures, and calls for a reassessment of seismic design criteria to enhance resilience in high-risk areas.	Binici et al. [46]
The 6 February 2023 earthquake sequence in Türkiye caused significant seismic impacts on 140 dams, with earthfill and rockfill dams near the fault rupture experiencing greater damage, including permanent deformations, particularly as their height increased.	Cetin et al. [47]
Presents findings from on-site geotechnical and structural investigations following the 6 February 2023 Kahramanmaraş earthquakes, highlighting severe damage to reinforced concrete, precast, and masonry structures, and identifying common deficiencies such as poor materials, inadequate construction techniques, and lack of engineering services.	Demir et al. [48]
Based on studies on post-earthquake damage assessment, the use of machine learning in decision support systems is explored.	Özman et al. [49]
Analyzes the factors contributing to structural damage during the February 2023 earthquakes in southeastern Türkiye, focusing on seismic characteristics, field observations, and key structural deficiencies.	Yön et al. [50]
Evaluates the impacts of the 6 February 2023 earthquakes on various structural systems in Kahramanmaraş, highlighting issues with soil–structure interaction, building materials, and the need for updates to earthquake code provisions.	Avcil et al. [51]
Proposes and validates a Rapid Damage Assessment (RDA) methodology using open data to estimate earthquake losses, applied to the 2023 Türkiye earthquakes, with the results closely aligning with official damage reports.	Apostolaki et al. [52]
Evaluates the damage to masonry village schools during the 2023 Kahramanmaraş earthquakes, analyzes their seismic performance, and proposes repair and strengthening recommendations.	Işık et al. [53]
Analyzes the seismic characteristics and structural damage caused by the February 2023 earthquakes in Kahramanmaraş, identifying key factors such as weak building design, poor construction quality, and unfavorable ground conditions.	Avgın et al. [54]
Examines the impact of the February 2023 earthquakes in Türkiye on various structures and infrastructure, providing insights for future seismic damage prevention and mitigation.	Yüzbaşı [55]
Analyzes the damage to industrial buildings from the February 2023 earthquakes in Türkiye, combining field observations and numerical analyses to assess structural integrity and highlight the importance of quality control in construction to improve seismic resilience.	Kirtel et al. [56]
Examines earthquake-related damage to reinforced concrete buildings in Malatya following the February 2023 Kahramanmaraş earthquakes, focusing on construction defects and their compliance with Turkish Earthquake Regulations.	Atar vd. [57]
Analyzes the seismic impact of the February 2023 earthquakes on Elazığ, Türkiye, examining tectonic, geological, and structural factors, and offering recommendations to prevent future damage and improve building practices.	Yetkin et al. [58]
Examines the liquefaction hazards in Hatay, Türkiye, following the February 2023 Kahramanmaraş earthquakes, highlighting the role of geological and geomorphological factors in liquefaction and lateral spreading in affected areas.	Bol et al. [59]
Evaluate the seismic performance and residual displacements of a base-isolated hospital under construction during the February 2023 Kahramanmaraş earthquakes, highlighting the impact of construction stages on structural vulnerability and damage probabilities.	Şen et al. [60]
Analyzes seismic characteristics and precursor patterns within the East Anatolian Fault System from 1983 to 2022, identifying trends that may have indicated the February 2023 earthquakes in Türkiye.	Trifonova et al. [61]
Develops a regression model to predict the seismic input energies of reinforced concrete buildings based on data from the February 2023 Kahramanmaraş earthquake, highlighting the effectiveness of acceleration-based parameters for low-period buildings.	Balun [62]

These studies attempt to reveal the characteristic features of earthquakes as well as their effects on the ground and different structural systems. While some of these studies take into account the entire earthquake region, others include smaller-scale evaluations within the scope of earthquake and civil engineering. In addition to studies based on observation, there are also studies in which structural analysis is carried out. This study is one of the first studies to carry out both seismic hazard and structural analyses by taking into account all settlements located on the EAFZ.

Ground motion parameters are essential to determine and evaluate the effects of earthquakes [63,64]. These parameters are important in revealing earthquake characteristics and analyzing the behavior of structures under the influence of earthquakes [65–67]. In determining ground motion parameters by taking into account local ground conditions, fault geometry, seismic waves, and earthquake characteristics should be known. Ground speed, acceleration, and displacement values are known as amplitude parameters [68–70]. Earthquake ground motion measurements are of critical importance for earthquake-resistant structural design, engineering applications, and scientific studies. Ground acceleration records obtained from strong ground motion measurements can be used both to determine seismic risk and to monitor the performance of the structures during earthquakes. Acceleration records are also used for the design of earthquake-resistant structures and the development of attenuation relationships. In addition, the expected damage estimate and density distribution in settlements at different distances from the station can be determined using attenuation relationships [71,72]. Therefore, PGA values obtained from any earthquake can be used to determine seismic and structural risks. In performance-based design, different types of analyses are used to decide on the performance levels of structures [73–76]. The main purpose of performance-based design is to determine the structural demand in structures affected by ground motion. The accurate determination of structural demand requires an accurate definition of ground motion characteristics and the relationship between them and structural demand [77,78]. The performance-based design methodology consists of four different stages, namely, determining the earthquake hazard and related seismic parameters, determining the structural analysis phase and related engineering parameters, measuring the predicted damage level, and making the necessary engineering decisions according to the damage levels [79]. The application of target displacement design in the context of performance-based earthquake engineering aims to estimate the performance of structures in earthquakes more accurately and safely. The amount of displacement (deformation) that will occur in the structural elements of the structures during an earthquake is one of the main factors affecting the structure's performance. It is attempted to keep these displacement values within a certain limit. One of the most important parameters in determining the performance levels is the target displacement. This is the maximum displacement of a control node that is likely to occur during the design earthquake. Different performance levels have different target displacements representing different seismic intensities [80–82].

One of the goals of earthquake-resistant structural design is to resist a possible earthquake effect without excessive damage. Determining target displacements for damage estimation when specific performance limitations of structural elements are met is crucial in performance-based earthquake engineering. When the displacement demand in the building is reached for a specific earthquake effect, it can be checked whether the expected performance target of the structure is achieved. The definition of acceptable damage limits aligns with the performance goals projected at different seismic levels [83–85]. Performance-based design's main goal is to ascertain the structural requirement in constructions susceptible to ground motion. The accurate description of ground motion features and their link to structural demand are necessary for the realistic determination of structural demand [86–88]. There are also various studies in the literature on target displacements in structures. Işık et al. [89] obtained the expected target displacement values from structures using five different earthquake datasets from six different countries. Işık [90] compared the displacements for instrumental period earthquake epicenters in Türkiye in his study. Bilgin et al. [91]

obtained the target displacement values by taking into account the minimum structural conditions for different countries.

In this study, firstly, information is given about the Kahramanmaraş earthquakes, which caused great destruction, and the EAFZ, which is the subject of the study. After providing information about the major earthquakes occurring in this fault zone, the PGAs used in Türkiye for the last two earthquake hazards for 20 different settlements located directly on this fault zone are compared. The main goal of this study is to first reveal whether the earthquake hazard is adequately represented for twenty different settlements located directly on the EAFZ, where the 2023 Türkiye earthquakes the disaster of the century for this country, occurred. For this purpose, the predicted values for the last two earthquake hazards used in Türkiye and the measured values from the earthquakes are compared for these settlements taken into consideration. Then, the impacts of the earthquake couple on RC structures are investigated within the scope of earthquake civil engineering. In the last part of the paper, pushover analyses are carried out for twenty different settlements located on the EAFZ for a sample RC structural model. For this purpose, separate structural analyses are performed for the measured Peak Ground Acceleration (PGA) for these settlements in both earthquakes and the predicted PGA in the last two earthquake hazard maps used in Türkiye. By comparing all the target displacement values obtained, it was attempted to reveal whether the displacements used in determining the earthquake performances of the structures were adequately represented. The most important aspect that distinguishes this study from other studies is this is a detailed study carried out for the first time for twenty different settlements located on the EAFZ. It is thought that this study, which is quite comprehensive in terms of both earthquake hazard and target displacements, will be a source for the development of seismic design regulations and earthquake maps. With the realistic and sufficient presentation of the earthquake hazard, the displacements to be used in determining the earthquake performance of the structures will be obtained much more accurately. With this study, both seismic and structural parameters were compared for all the settlements located directly on the EAFZ, which is one of the main tectonic elements of Türkiye, and it was attempted to reveal whether the earthquake hazard was adequately represented. Studies conducted after the Kahramanmaraş earthquakes generally reveal the effects of the earthquake on observation-based damage assessments and specifically selected structures. The difference of this study from other studies is that it reveals the predicted seismic hazard for all settlements on the EAFZ and whether it adequately represents the target displacements of the structures. In addition, this study compared the predicted seismic hazard values for the settlements on the EAFZ with the last two earthquake hazards used in Türkiye. The study also provides detailed information about many studies conducted on these earthquakes.

2. The EAFZ and 6th of February Kahramanmaraş Earthquakes

Türkiye is located in the Alpine–Himalayan earthquake zone, which is a high-seismic-risk region. The movement of the African Plate due to its counterclockwise rotation pushes the Arabian Block northward and the southeastern part of the Anatolian Block northward. In addition, the Anatolian Block is being pushed southward by the clockwise movement of the Eurasian Plate. For this reason, the Anatolian Block is under the impact of these two vital compressions and is shifting in the W-SW direction. The plate tectonic model of Anatolia and its surroundings are shown in Figure 1. As the main tectonic elements of Türkiye, the Northern Anatolian Fault Zone (NAFZ), the EAFZ, and the Aegean Graben System come to the fore due to the earthquakes that occur on them.

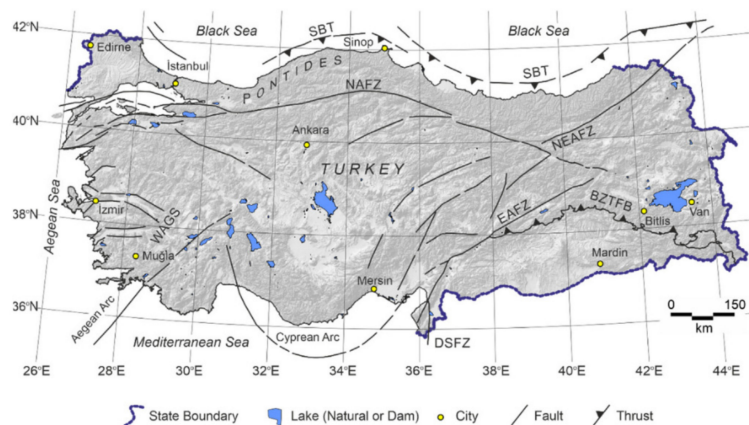


Figure 1. Simplified neotectonic and relief maps of Türkiye [92].

Finally, the 6 February 2023 Kahramanmaraş and the 2020 Elazığ earthquakes have drawn attention to the EAFZ. The EAFZ is Türkiye’s second major fault zone, which has produced earthquakes that have given rise to substantial loss of life and property throughout history. The East Anatolian Fault Zone, which has been the origin of many major earthquakes throughout history, had a very active period in the 1800s. It caused a sequence of earthquakes that began with the Antakya earthquake in 1822, proceeded to the earthquakes in 1866, 1872, 1874, 1875, and 1893, and ended with the Malatya earthquake in 1905. It went through a comparatively quieter phase following this earthquake and failed to produce an earthquake big enough to cause a surface break. It has been said that there has been a build-up of major pressures and that this stillness is just transitory [93–96].

The EAFZ is an NE-SE-oriented left-lateral slip fault that separates the Anatolian plate from the Arabian plate and is the left-lateral equivalent of the NAFZ. It merges with the Dead Sea Fault Zone near Türkoğlu and with the NAFZ near Karlıova. The zone consists of many complementary left-lateral strike-slip faults with various features between Karlıova and Antakya and is called the EAFZ [97,98]. The EAFZ is nearly 30 km wide and 700 km long with a ~10.5 mm/year slip rate value [99–102]. Table 3 displays significant historical and instrumental earthquakes on the EAFZ.

Table 3. Earthquakes on the EAFZ [103–108].

Historical Period			Instrumental Period		
Date	Region	Intensity	Date	Region	Magnitude
M.Ö. 148	Antakya	VIII	1905	Pütürge	$M_s = 6.8$
M.Ö. 69	Antakya	IX	1945	Ceyhan	$M_s = 6.0$
M.Ö. 37	Antakya	VIII	1952	Misis	$M_s = 5.6$
M.S. 53	Antakya	VIII	1964	Sincik	$M_s = 6.0$
220	Antakya	VII	1971	Bingöl	$M_s = 6.8$
396	Antakya	VIII	1975	Lice	$M = 6.6$
526	Antakya	IX	1979	Adana-Kozan	$M_s = 5.1$
529	Antakya	IX	1986	Sürgü	$M_w = 6.0$
1544	Elbistan	VIII	1991	Kadirli	$M_s = 5.2$
1738	Amik Lake	VIII	1994	Ceyhan	$M_s = 5.0$
1789	Elazığ	VIII	1997	Samandağ	$M_w = 5.7$
1822	Antakya	IX	1998	Yüreğir	$M_w = 6.2$
1872	Hatay	VIII–IX	2003	Bingöl	$M_w = 6.3$
1874	Elazığ	IX	2004	Sivrice	$M_w = 5.6$
1875	Elazığ	VI	2007	Sivrice	$M_w = 5.5$
1875	Palu		2007	Sivrice	$M_w = 5.7$
1893	Malatya	IX	2010	Kovanclar	$M_w = 6.1$

Since the beginning of 2020, destructive earthquakes have occurred in the EAFZ. On 24 January 2020, at 20:55:11 (17:55 GMT) local time, a damaging and shallow (12 ± 2 km) earthquake ($M_w = 6.8$) hit the Sivrice (Elazığ) province, with its epicenter on the Hazar–Sincik fault segment. The rupture area of this destructive earthquake was ~ 37 km long and the duration of the earthquake was found to be 20.4 s [109,110]. This earthquake caused 41 casualties with hundreds of injured people (~ 1607). The earthquake, with a recorded PGA value of 0.292 g, damaged $\sim 10,000$ buildings moderately or heavily or collapsed them [102,110–112]. These buildings can be generally classified as masonry dwellings, RC structures, and non-residential structures. The focal mechanism solution of the main shock is the pure left-lateral strike-slip fault (Figure 2). According to the AFAD earthquake catalog, ~ 2300 aftershocks with a magnitude bigger than $M_w \geq 2.0$ occurred in the region between 2020 and 2021 and the strongest aftershock had a magnitude of 5.0 Mw. Aftershocks occurred along Çelikhan–Gölbaşı, Gölbaşı–Türkoğlu and Palu–Hazar LakeHaza segments of the EAFZ in an SW-NE direction and it was consistent with the movement along with the EAFZ. The distribution of aftershocks consistently confirms the spread of seismicity along the ruptured fault [113]. After the Elazığ–Sivrice main shock, the Coulomb stress values were highly positive to the northeast and southwest of the 2020 rupture zone, especially at the increasing depth levels along the Gölbaşı–Türkoğlu and Türkoğlu–Antakya segments [102,114].

Following the 2020 Sivrice–Elazığ earthquake, two great earthquake doublets, described as the disasters of the century for Türkiye, occurred in the Pazarçık and Elbistan with a magnitude of $M_w = 7.7$ and 7.6, respectively, in the districts of Kahramanmaraş city on 6 February 2023. The first earthquake ($M_w = 7.7$) occurred in Pazarçık province at local time 04:17:32 (01:17 GMT) (Figure 2). This event ruptured ~ 310 km of the primary fault segments in harmony with a slightly left-lateral strike-slip fault mechanism along the northeast–southwest direction, namely, in Amanos, Pazarçık, and Erkenek, which caused a maximum fault slip of ~ 8 m and a hypocenter depth of 8.9 km. After 9 h, at a distance of 95 km from the $M_w = 7.7$ event, the second earthquake ($M_w = 7.6$) struck in Elbistan province at local time 10:51:28 (13:51 GMT), rupturing a ~ 150 km long fault trending left-lateral segments called the Göksun fault, Sürgü fault, Çardak fault, and Maraş fault on a roughly east–west orientation. The hypocenter depth of the second earthquake was 7.7 km [115–118]. These powerful earthquake pairs triggered a series of aftershocks in the region. On 20 February, a third earthquake ($M_w = 6.4$) struck the region of the Defne province (Hatay) graben near the Amanos segment. The Kahramanmaraş earthquakes and their aftershocks caused great structural damage in the Kahramanmaraş, Hatay, Gaziantep, Malatya, Diyarbakır, Kilis, Şanlıurfa, Adıyaman, Osmaniye, Adana, and Elazığ provinces. More than 40,000 buildings collapsed and over 200,000 buildings were affected or heavily damaged in the region. These devastating earthquakes caused over 60,000 deaths and 115,000 injuries in south-central Türkiye and northwestern Syria. More than 10 million people suffered from these deadly earthquakes [52,115,119,120]. A total of approximately 75,000 aftershocks occurred between February 2023 and August 2024 and aftershock distributions associated with these destructive doublet earthquakes have continued, especially along the DSFZ and NE of the EAFZ, as shown in Figure 2. The aftershock magnitudes were mostly between 1.0 and 4.9. Also, there were 61 large aftershocks ($M_w \geq 5.0$) in this period (AFAD, 2023) [119]. The hypocentre depths of the aftershocks varied between 5 km and 20 km depth, in general [118]. Considering the aftershock distributions, the positive stress fields are observed in the direction of the northern DSFZ in the southwest, as well as the Palu segment and Pütürge segment in the northwest [39,121].

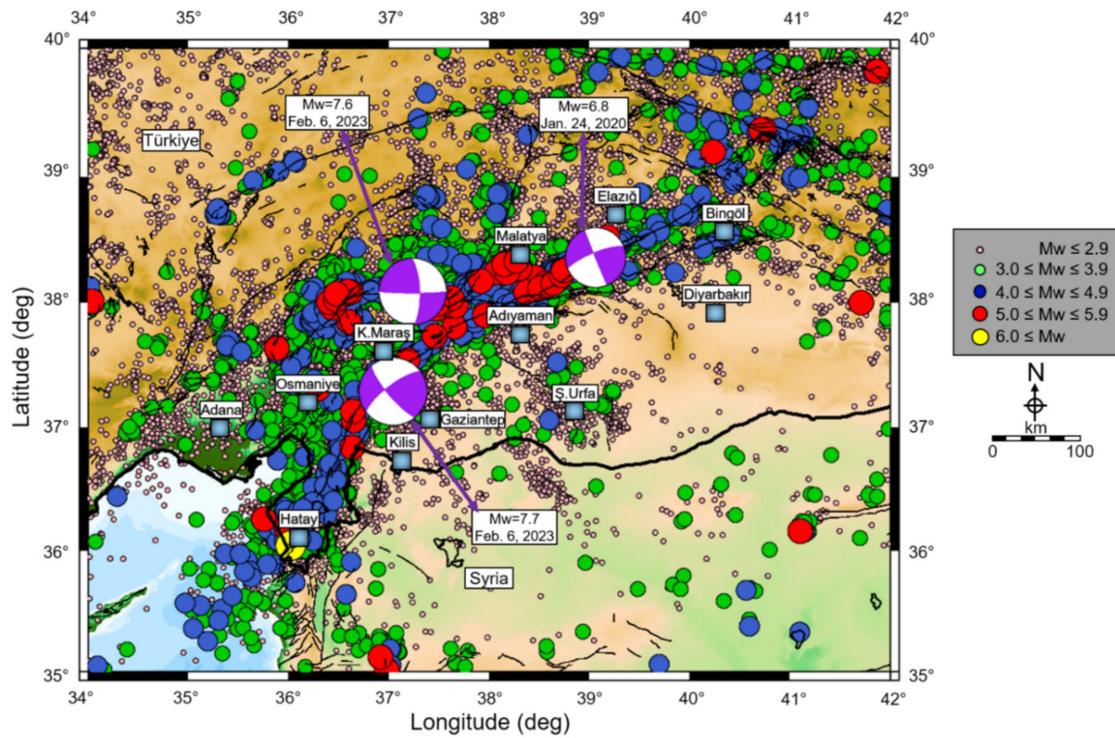


Figure 2. Epicenter locations of approximately 88,900 earthquakes with $1.0 \leq M_w \leq 7.9$ from 1 January 2020 to 1 August 2024. The seismicity catalog is obtained from the AFAD website [122]. Magnitude grades of the events are plotted with various circular symbols. Purple beach balls represent fault mechanism solutions of the 2020 Sivrice, 2023 Pazarcık, and Elbistan earthquakes. Black lines represent the locations of active faults taken from Emre et al. [123].

The distribution of damage by province from the damage assessment studies carried out by the relevant Ministry until 6 March 2023 following the 2023 Kahramanmaraş earthquakes is given in Table 4.

Table 4. Damage assessment report by province (6 March 2023) [124].

Province	Total Demolished Immediately + Heavily Damaged + Collapsed Residential Buildings	Moderate Damaged	Slightly Damaged
Adana	2952	11,768	71,072
Adiyaman	56,256	18,715	72,729
Diyarbakır	8602	11,209	113,223
Elazığ	10,156	1522	31,151
Gaziantep	29,155	20,251	236,497
Kahramanmaraş	99,326	17,887	161,137
Malatya	71,519	12,801	107,765
Hatay	215,255	25,957	189,317
Kilis	2514	1303	27,969
Osmaniye	16,111	4122	69,466
Şanlıurfa	6163	6041	199,401
Total of the region	518,009	131,576	1,279,727

The instrumental period earthquake activity continued with the 2020 Elazığ (Sivrice) and 2023 Kahramanmaraş earthquakes. All of these statistical data clearly show that quite large and destructive earthquakes occurred in this fault zone. Hatay, Bingöl, Elazığ, Malatya, Kahramanmaraş, Osmaniye, Adıyaman, and their associated centers are the settlements nearest to this fault zone. The settlement centers located directly on the EAFZ are shown in Figure 3.

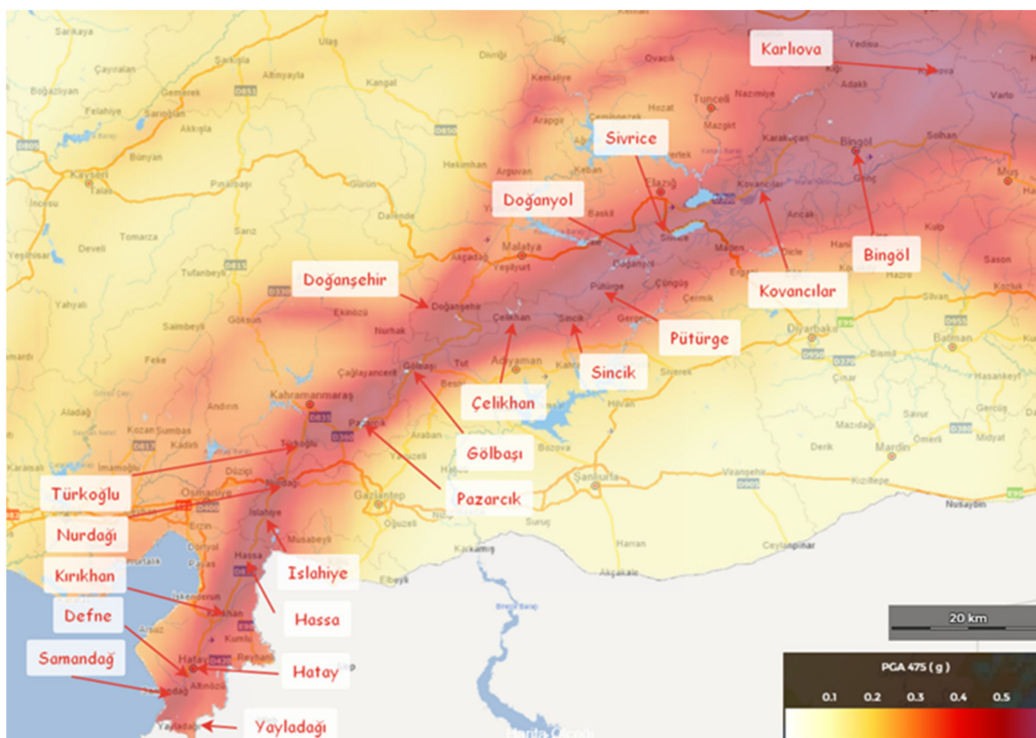


Figure 3. Settlements on the EAFZ within the scope of this study.

The Earthquake Zones Map, which has been used in Türkiye since 1996, has been replaced by the Türkiye Earthquake Hazard Map, which came into force with the Türkiye Building Earthquake Regulation (TBEC-2018) [125], as of 1 January 2019. In this paper, seismic parameters were compared using these two maps. In the current map, seismic parameters for any geographical location could be attained with the help of the Türkiye Earthquake Hazard Maps Interactive Web Application (<https://tdth.afad.gov.tr> accessed on 15 June 2024) [126]. While the previous map included only the standard design earthquake ground motion (recurrence period of 475 years) for the earthquake ground motion level, the current earthquake code expresses four different earthquake ground motion levels. Table 5 lists the earthquake ground motion levels that were used in the investigation.

Table 5. Earthquake ground motion levels [125].

Earthquake Ground Motion Level	Repetition Period (Year)	Probability of Exceedance (50 Years)	Definition
DD-1	2475	0.02	Largest earthquake
DD-2	475	0.10	Standard design ground motion
DD-3	72	0.50	Frequent earthquake ground motion level
DD-4	43	0.68	Service earthquake ground motion level

While obtaining seismic parameters for settlements directly located on the EAFZ and significantly affected by the February 6 Kahramanmaraş earthquakes, the average local soil ZC class in the current seismic design code was taken into consideration. In order to make comparisons, the same local soil class was not selected as a variable in all the settlements. The PGA, peak ground velocity (PGV), and design spectral acceleration coefficients (S_{DS}) were obtained for each randomly selected geographical location in the settlements. The PGA and PGV obtained for different earthquake ground motion levels for the locations are given in Table 6. The data start from the Yayladağı district of Hatay province and end in Karlıova, where the EAFZ ends.

Table 6. The predicted PGA and PGV for selected locations in the current earthquake hazard map.

No	Location	PGA (g)				PGV (cm/s)			
		DD-1	DD-2	DD-3	DD-4	DD-1	DD-2	DD-3	DD-4
1	Yayladağı	0.685	0.372	0.135	0.092	43.425	22.368	7.444	5.051
2	Samandağ	0.915	0.471	0.146	0.096	56.570	28.449	8.032	5.295
3	Defne	0.927	0.466	0.148	0.099	59.613	28.905	8.325	5.558
4	Hatay	0.877	0.448	0.148	0.100	56.243	27.757	8.339	5.592
5	Kırkhan	1.003	0.515	0.155	0.103	66.041	32.617	8.893	5.812
6	Hassa	1.137	0.602	0.175	0.110	76.387	39.603	10.026	6.112
7	Islahiye	1.048	0.554	0.164	0.107	67.984	34.890	9.444	5.990
8	Nurdağı	0.959	0.491	0.156	0.105	63.330	31.247	9.019	5.921
9	Türkoğlu	0.898	0.469	0.156	0.105	60.401	30.177	9.021	5.933
10	Pazarcık	0.939	0.516	0.170	0.106	71.517	37.627	9.803	5.957
11	Gölbasi	0.954	0.510	0.170	0.111	63.496	32.741	9.762	6.069
12	Doğanşehir	0.892	0.478	0.159	0.102	56.451	29.559	9.276	5.620
13	Çelikhan	1.062	0.592	0.209	0.126	78.014	42.002	11.316	6.379
14	Sincik	1.160	0.643	0.217	0.135	75.494	40.871	11.559	6.592
15	Pütürge	1.189	0.676	0.241	0.145	85.717	47.700	12.994	7.063
16	Doğanyol	1.158	0.663	0.250	0.151	88.852	49.597	13.670	7.456
17	Sivrice	1.139	0.645	0.232	0.146	81.334	43.944	12.880	7.466
18	Kovancılar	1.110	0.640	0.244	0.151	81.254	45.672	14.177	8.043
19	Bingöl	1.134	0.653	0.273	0.179	76.531	42.943	15.559	9.595
20	Karlıova	1.335	0.794	0.351	0.201	100.279	60.379	20.988	10.521

Considering these values, the lower and upper PGA and PGV for the located settlements directly on the EAFZ are shown in Table 7.

Table 7. Lower and upper PGA–PGV values of the settlement.

Earthquake Ground Motion Level	PGA (g)	PGV (cm/s)
DD-1	0.68–1.40	43–101
DD-2	0.37–0.80	22–61
DD-3	0.13–0.36	7–21
DD-4	0.09–0.21	5–11

In addition, the comparison of the PGA and design spectral acceleration coefficients (S_{DS}) for the last two earthquake hazards used in Türkiye is given in Table 8. To make

comparisons, the DD-2 ground motion level in both seismic design codes was taken into account.

Table 8. Comparison of PGA and S_{DS} for settlements on the last two earthquake hazard maps.

No	Location	Earthquake Region	1996	2018	2018/1996	S_{DS2007}	S_{DS2018}	S_{DS2018}/S_{DS2007}
			PGA (g)	PGA (g)				
1	Yayladağı	I	0.4	0.372	0.93	1	1.061	1.061
2	Samandağ	I	0.4	0.471	1.18	1	1.322	1.322
3	Defne	I	0.4	0.466	1.17	1	1.315	1.315
4	Hatay	I	0.4	0.448	1.12	1	1.266	1.266
5	Kırıkhan	I	0.4	0.515	1.29	1	1.447	1.447
6	Hassa	I	0.4	0.602	1.51	1	1.715	1.715
7	Islahiye	I	0.4	0.554	1.39	1	1.56	1.56
8	Nurdağı	I	0.4	0.491	1.23	1	1.396	1.396
9	Türkoğlu	I	0.4	0.469	1.17	1	1.345	1.345
10	Pazarcık	I	0.4	0.516	1.29	1	1.484	1.484
11	Gölbaşı	I	0.4	0.51	1.28	1	1.46	1.46
12	Doğanşehir	I	0.4	0.478	1.20	1	1.363	1.363
13	Çelikhan	I	0.4	0.592	1.48	1	1.702	1.702
14	Sincik	I	0.4	0.643	1.61	1	1.866	1.866
15	Pütürge	I	0.4	0.676	1.69	1	1.97	1.97
16	Doğanyol	I	0.4	0.663	1.66	1	1.927	1.927
17	Sivrice	I	0.4	0.645	1.61	1	1.877	1.877
18	Kovancılar	I	0.4	0.64	1.60	1	1.867	1.867
19	Bingöl	I	0.4	0.653	1.63	1	1.926	1.926
20	Karlıova	I	0.4	0.794	1.99	1	2.35	2.35

All settlements considered in the previous earthquake zone map are located in the 1° earthquake zone and the same PGA (0.400 g) is predicted. However, since geographical location-specific seismic parameters are predicted in the current earthquake hazard map, different PGAs are obtained for each settlement. With the current earthquake hazard map, the predicted PGAs for the same earthquake motion level have increased in all settlements except Yayladağı. The highest increase was in Karlıova district, while the lowest increase was in Hatay. Also, while the horizontal design elastic spectrum coefficient (S_{DS}) had the same value (1.00) in the previous earthquake zone map for the same local soil conditions and the same ground motion level, it had different values in the current earthquake hazard map. There was an increase in this coefficient in all the settlements. The highest increase was in Karlıova, while the lowest increase was in Yayladağı. The increase in both the PGA and S_{DS} values clearly reveals the reality of earthquakes in the EAFZ and the extent of the hazard.

Within the scope of this study, the obtained PGAs in both the earthquakes in the settlements were compared with the predicted PGAs in the last two earthquake hazard maps. It was attempted to reveal whether the earthquake hazard was adequately represented. The comparison of the measured (TADAS, 2023) [127] and predicted PGAs in the settlements in the first earthquake, the Pazarcık earthquake, is given in Table 9. Table 9 also compares the predicted PGAs for the standard design ground motion level DD-2 in the current earthquake hazard map with the values predicted for the maximum earthquake ground motion level (DD-1) for the settlements where the measured PGAs exceed.

Table 9. Comparison of measured PGAs of Pazarcık ($M_w = 7.7$) with the last two earthquake hazard maps.

No	Location	Pazarcık Earthquake	TSDC-2007		TBEC-2018		TBEC-2018	
			PGA (g) DD-2	Provide or Not	PGA (g) DD-2	Provide or Not	DD-1	Provide or Not
1	Yayladağı	0.048	0.400	✓	0.372	✓	0.685	✓
2	Samandağ	0.223	0.400	✓	0.471	✓	0.915	✓
3	Defne	1.378	0.400	X	0.466	X	0.927	X
4	Hatay	1.201	0.400	X	0.448	X	0.877	X
5	Kırıkhan	0.754	0.400	X	0.515	X	1.003	✓
6	Hassa	1.322	0.400	X	0.602	X	1.137	X
7	Islahiye	0.667	0.400	X	0.554	X	1.048	✓
8	Nurdağı	0.604	0.400	X	0.491	X	0.959	✓
9	Türkoglu	0.367	0.400	✓	0.469	✓	0.898	✓
10	Pazarcık	2.222	0.400	X	0.516	X	0.939	X
11	Gölbaşı	0.031	0.400	✓	0.510	✓	0.954	✓
12	Doğanşehir	0.140	0.400	✓	0.478	✓	0.892	✓
13	Çelikhan	0.071	0.400	✓	0.592	✓	1.062	✓
14	Sincik	0.129	0.400	✓	0.643	✓	1.160	✓
15	Pütürge	0.018	0.400	✓	0.676	✓	1.189	✓
16	Doğanyol	0.018	0.400	✓	0.663	✓	1.158	✓
17	Sivrice	0.050	0.400	✓	0.645	✓	1.139	✓
18	Kovancılar	0.050	0.400	✓	0.640	✓	1.110	✓
19	Bingöl	0.004	0.400	✓	0.653	✓	1.134	✓
20	Karlıova	0.016	0.400	✓	0.794	✓	1.335	✓

The predicted PGAs for DD-2 in the last two earthquake hazard maps used in Türkiye exceeded the values measured in Defne, Hatay, Kırıkhan, Hassa, Islahiye, Nurdağı, and Pazarcık in the Pazarcık earthquake. The predicted values in the other settlements remained below the recommended values. On the other hand, the predicted PGAs for the largest earthquake (DD-1) in the current earthquake hazard map was exceeded in the Defne, Hatay, Hassa, and Pazarcık districts. The reason for this is that the EAFZ has been silent for a very long time and has not produced a large earthquake. At the same time, these earthquakes are the largest earthquakes that have occurred on the EAFZ in the instrumental period. Therefore, updating the seismic hazard analyses for the settlements located on the EAFZ by taking these earthquakes into account will allow the earthquake hazard of the region to be presented more realistically.

Within the scope of this study, the comparison of the predicted and measured PGAs for the second earthquake, which occurred 9 h after the first earthquake on the EAFZ and whose epicenter was the Elbistan district of Kahramanmaraş province, is given in Table 10. For settlements where no measurement values could be reached, the highest values measured in the settlements closest to these settlements were taken into account.

The measured values in the second earthquake, that in Elbistan (Kahramanmaraş), exceeded only the predicted value for Doğanşehir in the previous earthquake zone map. In the current earthquake hazard map, the values predicted for the ground motion level generally used in the design of structures in all the settlements were not exceeded in any settlement. This shows that the current earthquake hazard map is sufficiently represented for this earthquake. Since there was no measurement value in the Sincik, Pütürge, and Sivrice districts for this earthquake, the value measured in Çelikhan, another district closest to this area, was taken into account for Sincik. For the Pütürge, Doğanyol, and Sivrice districts, the highest value measured in the Kovancılar district was taken into account.

Since there was no measurement value in the Gölbaşı, Çelikhan, and Sincik districts of the Adıyaman province due to the second earthquake, the highest value measured in the Tut district of Adıyaman province, which was 0.129 g, was taken into account for this earthquake. For the Nurdağı district, the highest value measured in the Gaziantep province, to which the district is affiliated, was taken into account. The highest measured value in the Akçadağ district, which is the closest district to the Doğanşehir district, was taken into account, which was 0.476 g. The value measured in the Sivrice district of Kovancılar, which is another district where no measurement was made, was taken into account.

Table 10. Comparison of the measured PGAs of Elbistan ($M_w = 7.6$) earthquake.

No	Location	Elbistan Earthquake	TSDC-2007	Provide or Not	TBEC-2018	Provide or Not
			PGA (g) DD-2		PGA (g) DD-2	
1	Yayladağı	0.005	0.400	✓	0.372	✓
2	Samandağ	0.031	0.400	✓	0.471	✓
3	Defne	0.027	0.400	✓	0.466	✓
4	Hatay	0.033	0.400	✓	0.448	✓
5	Kırıkhan	0.059	0.400	✓	0.515	✓
6	Hassa	0.070	0.400	✓	0.602	✓
7	Islahiye	0.052	0.400	✓	0.554	✓
8	Nurdağı	0.096	0.400	✓	0.491	✓
9	Türkoğlu	0.059	0.400	✓	0.469	✓
10	Pazarcık	0.210	0.400	✓	0.516	✓
11	Gölbaşı	0.129	0.400	✓	0.510	✓
12	Doğanşehir	0.476	0.400	X	0.478	✓
13	Çelikhan	0.129	0.400	✓	0.592	✓
14	Sincik	0.129	0.400	✓	0.643	✓
15	Pütürge	0.049	0.400	✓	0.676	✓
16	Doğanyol	0.052	0.400	✓	0.663	✓
17	Sivrice	0.071	0.400	✓	0.645	✓
18	Kovancılar	0.071	0.400	✓	0.640	✓
19	Bingöl	0.010	0.400	✓	0.653	✓
20	Karlıova	0.006	0.400	✓	0.794	✓

3. Damage Observed in RC Structures

The disaster of the century for Türkiye, the earthquakes centered in Kahramanmaraş on 6 February 2023, caused great destruction in a very large region. In addition to the large-scale loss of life and property resulting from the destruction, there were economic losses that the country could not handle. In addition, the damage to transportation structures caused a loss of time in necessary aid and interventions. However, the interventions made in these structures in a very short time and the rapid establishment of alternative routes solved this problem in a short time. The earthquake caused destruction and structural damage at different levels in different structural systems. In the region, very great destruction also occurred in reinforced concrete buildings, which are the main urban building stock. In this study, RC structures located in the settlements considered and exposed to various levels of structural failure were evaluated observationally by taking into account the damage. Examples of RC buildings that have received various levels of structural damage in different settlements as a consequence of field examinations are shown in Figure 4.



Figure 4. RC structures exposed to various levels of structural damage.

Pre-earthquake and post-earthquake images and schematic representations of this damage for two sample RC buildings are shown in Figure 5. Pre-earthquake images were taken with the help of Google Street View.

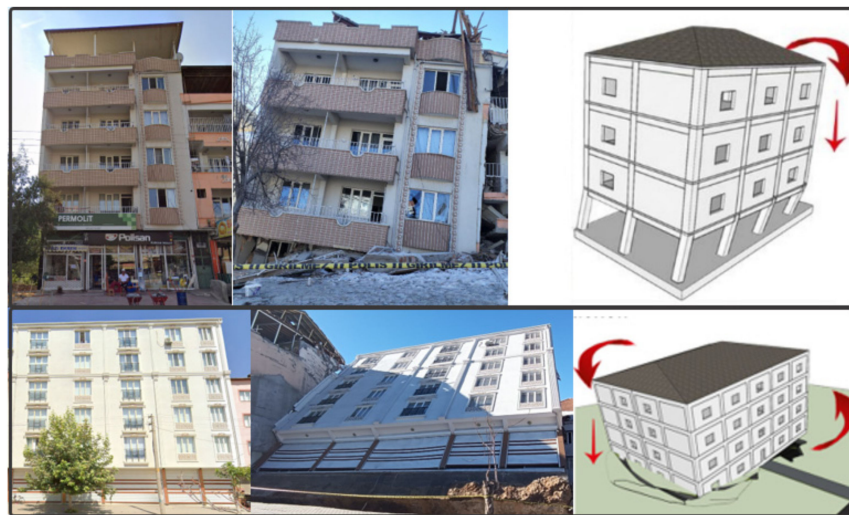


Figure 5. Pre-earthquake and post-earthquake images of two sample RC structures.

Examples of RC buildings in the earthquake region where life safety was ensured despite damage to nearby structures are shown in Figure 6.



Figure 6. Examples of RC buildings with life safety ensured. (a) RC building standing despite the collapse of neighboring buildings, (b) example of RC building for pre-collapse performance level, and (c) example of a completed but not yet occupied building without damage.

The damage to the RC buildings in the settlements and their schematic damage representations are given in Figure 7.


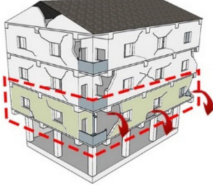

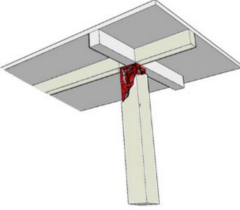

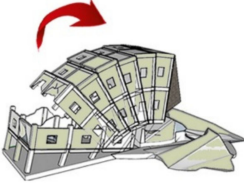

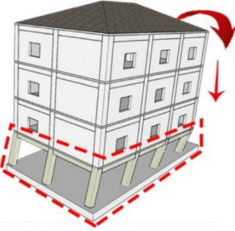

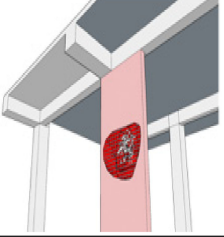

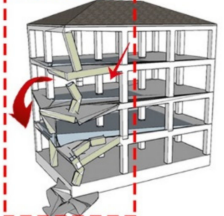
No	Damage	Schematic Representation	Damage Reason
1			Heavy overhang
2			The plastic hinge of the corner column upper region
3			Lateral collapse (accordion) damage
4			Total collapse due to soft storey on the ground storey
5			Improper aggregate granulometry and usage of flat reinforcement
6			Inadequate RC frame; lack of interlocking between slab-beam-column

Figure 7. Cont.

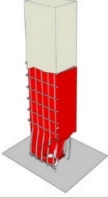

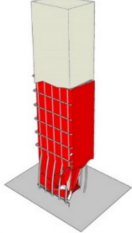
7			Soft storey
8			Insufficient transverse reinforcement in the beam–column joint
9			Usage of excessive reinforcement
10			Shear damage in RC shear wall
11			Rupture in transverse reinforcement
12			Pounding effect
13			Short column damage due to band-type window
14			Buckling damage in longitudinal steel rebar due to insufficient transverse reinforcement

Figure 7. Cont.




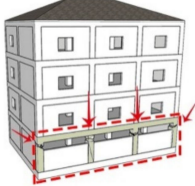

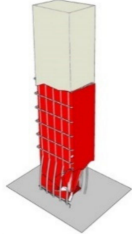

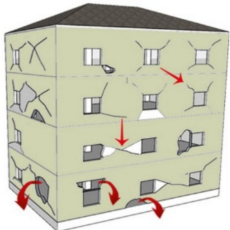

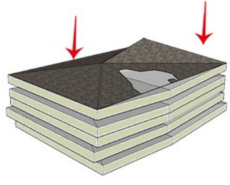

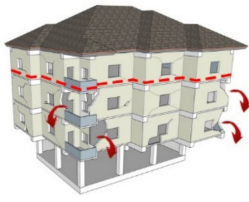


15			Corrosion of the reinforcement/lack of concrete cover
16			Short column damage because of band-type window
17			Insufficient transverse reinforcement
18			Shear damage in infill walls
19			Pancake collapse example because of inadequate RC frame; strong beam–weak column
20			Torsion damage in a structure with irregularity in the plan
21			90° hooks instead of 135°

Figure 7. Cont.




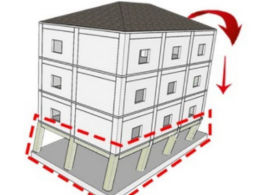

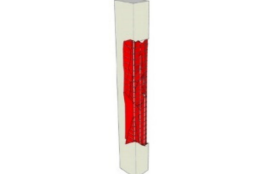

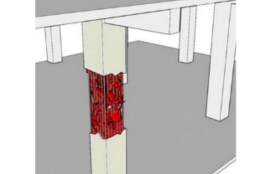

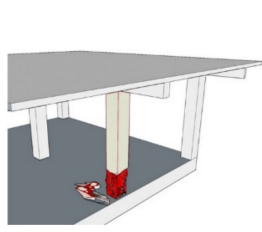
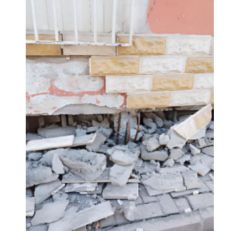
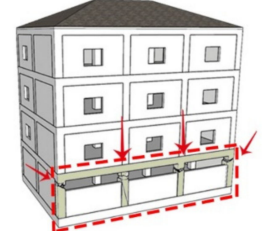
22			Out-of-plane failure damage of infill walls
23			Partial collapse damage due to soft storey
24			Lack of concrete cover
25			Improper aggregate granulometry
26			Insufficient transverse reinforcement; plastic hinges in structural elements
27			Band-type short column

Figure 7. Observed damage and its schematic representations.

When the damage observed in the RC structures is examined, one or more factors such as soft/weak storeys, short columns, strong beam–weak column application, insufficient interlocking between RC frame elements, low-strength concrete, poor workmanship, insufficient reinforcement, torsion effect in structures with irregularity in plan, closed heavy overhangs in structures, insufficient concrete cover thickness, usage of low-strength infill wall material, poor infill wall workmanship, inappropriate aggregate granulometry, and a pounding effect in neighboring structures are the main reasons for the damage. Irregularities in structures and the incomplete or incorrect application of earthquake-resistant structural design principles have caused an increase in damage. In this context, it should not be forgotten that structures where earthquake-resistant structural design principles are applied both in the construction and project stages provide a life safety performance level and prevent an increase in casualties. When evaluated from this perspective, the

design of RC structures that is as simple as possible, transferring the loads that will affect the structure to the ground easily and containing as little irregularity as possible will play a critical role in increasing the earthquake performance of such structures. In addition to the damage causes considered in this study, it is also important to adequately represent the earthquake magnitude taken into account in the design of the structure. Design spectra obtained without adequate representation do not allow one to realistically obtain the damage and performance of structures under the effect of earthquakes. Within the scope of this study, it was attempted to reveal whether the effect of earthquake hazards on structures was adequately represented for all the settlements located on the EAFZ where the 2023 Kahramanmaraş earthquakes occurred. For this purpose, target displacements were compared over the created structural model.

4. Comparison of Target Displacements in Performance-Based Earthquake Engineering

The threat that earthquakes pose to human activities in many parts of the world is reason enough to carefully consider earthquakes in the design of structures and facilities. The goal of earthquake-resistant design is to construct structures and facilities that can withstand a certain level of shaking without excessive damage. Structural analyses were performed to compare the target displacement values of the earthquakes considered. Structural analyses were performed separately with Seismostruct [128] for all the obtained PGAs in this study. Pushover analyses were carried out for a sample RC structural model, taking into account the PGAs. The sample RC numerical model is seven-storey, and the storey heights are equal, all being 3 m. The structure is symmetrical and has equal openings in the X and Y directions, and each opening is selected as 4.50 m. The 2D and 3D models and applied loads created in the software for the selected sample RC structure are shown in Figure 8.

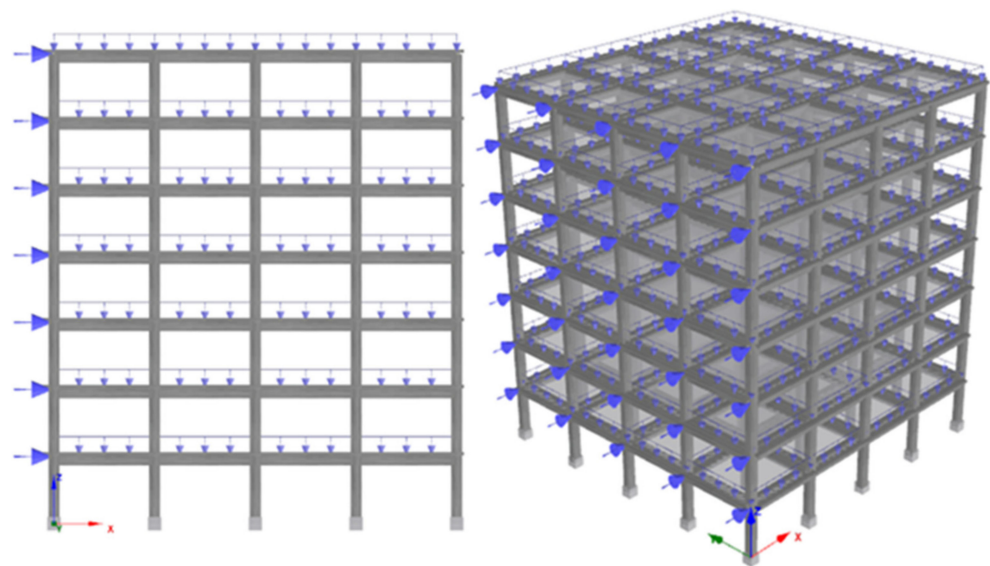


Figure 8. Two-dimensional and three-dimensional models of the RC structure.

For every structural model, 0.42 m was chosen as the target displacement value. ZC, the typical soil class in Eurocode-8, was selected as the local soil class. The properties of this type of soil class are given in Table 11.

Table 11. Properties of local soil classes [129].

Ground Type	Description of Stratigraphic Profile	V_s , 30 (m/s)	Parameters NSPT (Blows/30 cm)	C_u (kPa)
ZC	Deep deposits of dense or medium-dense sand, gravel, or stiff clay with thickness from several tens to many hundreds of meters.	180–360	15–50	70–250

All the building models were formed using the infrastructure FBPH (force-based plastic hinge frame elements) for structural parts like beams and columns. These components restrict plasticity to a finite length and simulate force-based extensional flexibility. To accurately represent the stress–strain distribution in the section, the optimal number of fibers in the section should be sufficient [130]. Consideration of the nonlinear behavior of the material is made possible by the definition of the plastic hinge. For the chosen sections, a total of one hundred fiber elements have been defined. For certain kinds of divisions, this value suffices. The selected plastic hinge length (L_p/L) was 16.67%. Damage estimation is successful to the extent that the plastic hinge parameters and deformation limit states reflect the actual structure behavior. In order to determine the earthquake performance of the structure, plastic hinge definitions must be made for structural elements and the extent of damage that will occur in structural elements under which cross-sectional effects must be predicted. Plastic hinge parameters and deformation limit values have been determined with various standards in structural design and existing structure evaluation [131–133].

Setting the column’s boundary conditions in accordance with the cantilever boundary requirements resulted in a fully fixed column footing and a free top end. The footings’ border condition was set in place. Figure 9 displays the sample storey formwork plan for the model of the RC building. Table 12 displays the RC structural model features that were considered throughout the structural analysis.

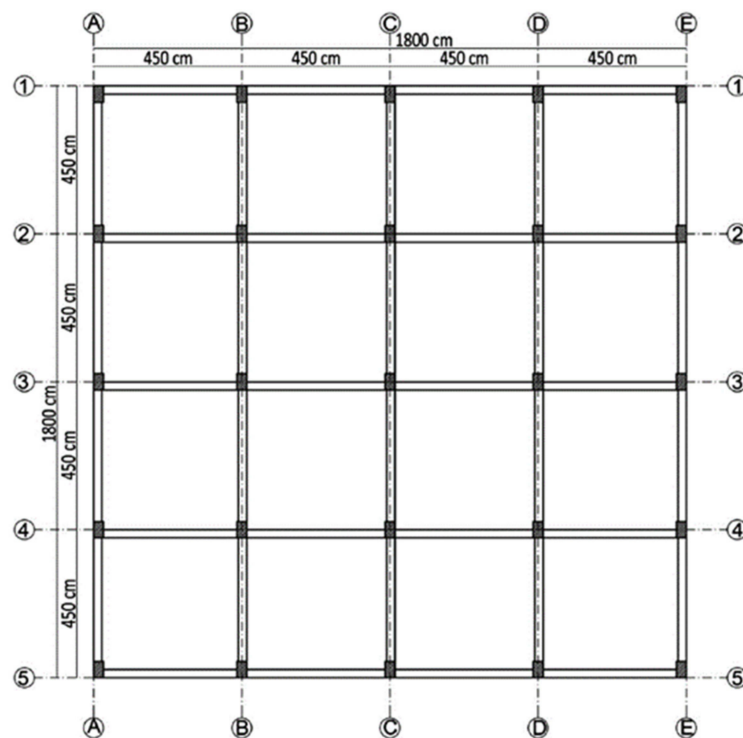


Figure 9. The storey formwork plan for the sample RC building.

Table 12. RC structural model’s characteristics.

Parameters		Values	Parameters	Values
Concrete		C25	Stirrup (columns)	Φ8/100
Reinforcement		S420	Stirrup (beam)	Φ8/150
Beam (mm)		250 × 600	Steel material model	Menegotto–Pinto
Height of slab (mm)		120	Constraint type	Rigid diaphragm
Height of each storey (m)		3	Concrete material model	Nonlinear (Mander et al.)
Cover thickness (mm)		25	Local ground type	ZC
Columns (mm)		400 × 500	Incremental load	5 kN
Longitudinal reinforcement (columns)	Corners	4Φ20	Dead load	5 kN/m
	Top bottom side	4Φ16	Damping	5%
	Left right side	4Φ16	Importance class	III

In performance-based earthquake engineering, identifying the objective displacements for damage estimation is essential when specific structural member performance limits are reached. The limit states provided in Eurocode-8/Part 3 [129,134] were taken into account in the structural analysis for damage estimation that is utilized globally. Figure 10 displays all of these displacements. The software lists three distinct scenarios for the damage cases. These are regarded as damage limitation (DL), significant damage (SD), and near collapse (NC). Every structural model has these values computed. Table 13 provides comprehensive descriptions of various limit states.

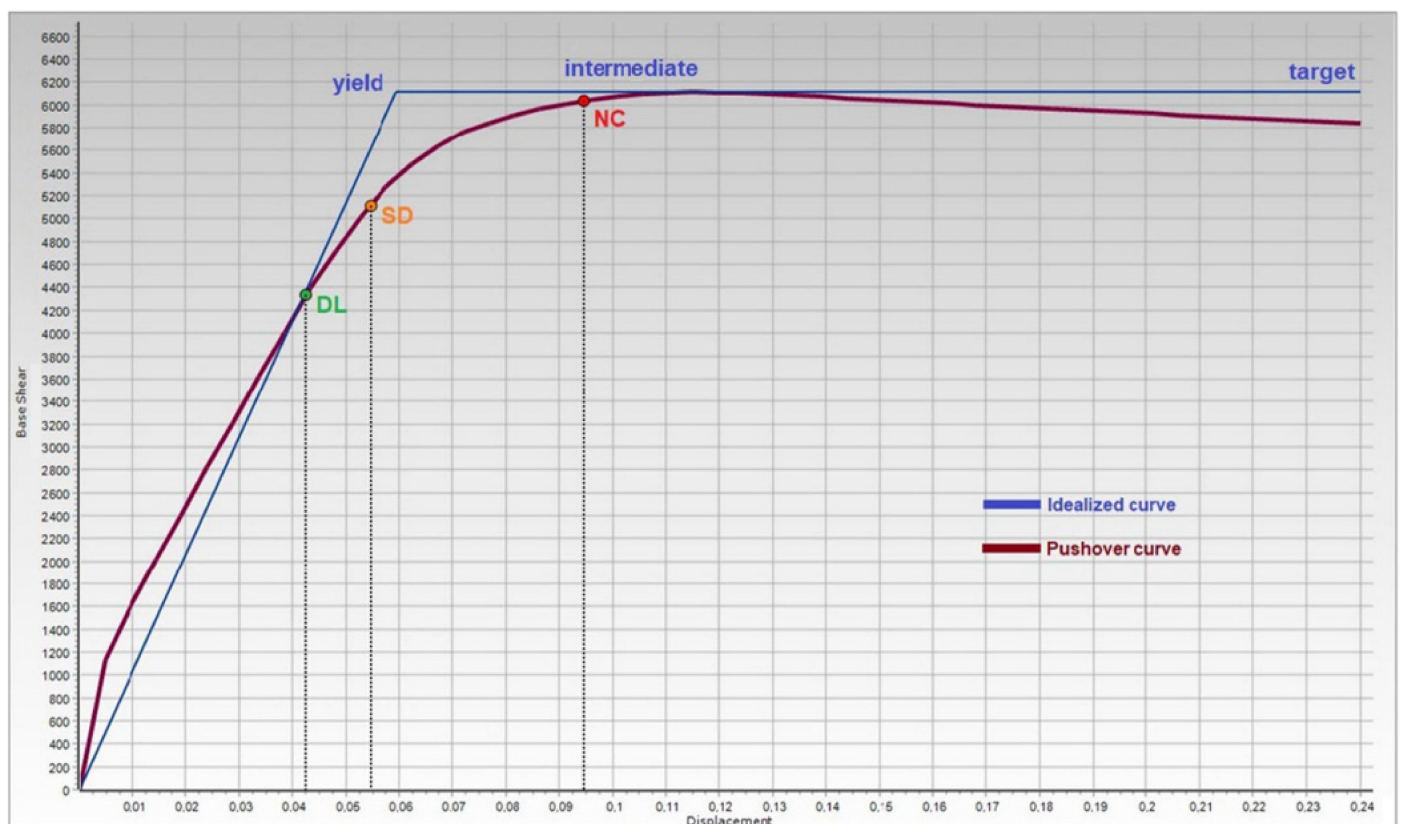


Figure 10. Standard pushover, idealized curves, and target displacements.

Table 13. Limit states in Eurocode 8/Part 3 [129,134].

Limit State	Description	Return Period (Year)	Probability of Exceedance (in 50 Years)
Damage limitation (DL)	Only lightly damaged; damage to non-structural components is economically repairable	225	0.20
Significant damage (SD)	Significantly damaged; some residual strength and stiffness; non-structural components damaged; uneconomic to repair	475	0.10
Near-collapse (NC)	Heavily damaged; very low residual strength and stiffness; large permanent drift but still standing	2475	0.02

Under the previous seismic design code, structural assessments were first carried out for the ground motion level with a probability of exceedance for the standard design earthquake of 10% (repetition period 475 years) in 50 years. All the structural analysis results are displayed in Table 14 and include limit states for the measured PGAs, the present code, and the preceding code, which were all obtained individually.

Table 14. Comparison of measured with predicted limit states for the Pazarcık earthquake.

No	Location	Limit States (m)								
		Measured PGA			TSDC-2007			TBEC-2018		
		DL	SD	NC	DL	SD	NC	DL	SD	NC
1	Yayladağı	0.019	0.024	0.042	0.158	0.202	0.351	0.147	0.188	0.326
2	Samandağ	0.088	0.113	0.196	0.158	0.202	0.351	0.186	0.238	0.413
3	Defne	0.543	0.697	1.208	0.158	0.202	0.351	0.184	0.236	0.409
4	Hatay	0.474	0.608	1.053	0.158	0.202	0.351	0.177	0.227	0.393
5	Kırıkhan	0.297	0.381	0.661	0.158	0.202	0.351	0.203	0.261	0.452
6	Hassa	0.521	0.669	1.159	0.158	0.202	0.351	0.237	0.305	0.528
7	Islahiye	0.263	0.337	0.585	0.158	0.202	0.351	0.218	0.280	0.486
8	Nurdağı	0.238	0.306	0.530	0.158	0.202	0.351	0.194	0.248	0.431
9	Türkoğlu	0.145	0.186	0.322	0.158	0.202	0.351	0.185	0.237	0.411
10	Pazarcık	0.876	1.124	1.949	0.158	0.202	0.351	0.203	0.261	0.452
11	Gölbaşı	0.012	0.016	0.027	0.158	0.202	0.351	0.201	0.258	0.447
12	Doğanşehir	0.055	0.071	0.123	0.158	0.202	0.351	0.188	0.242	0.419
13	Çelikhan	0.028	0.036	0.062	0.158	0.202	0.351	0.233	0.299	0.519
14	Sincik	0.051	0.065	0.113	0.158	0.202	0.351	0.254	0.325	0.564
15	Pütürge	0.007	0.009	0.016	0.158	0.202	0.351	0.267	0.342	0.593
16	Doğanyol	0.007	0.009	0.016	0.158	0.202	0.351	0.261	0.335	0.581
17	Sivrice	0.020	0.025	0.044	0.158	0.202	0.351	0.254	0.326	0.566
18	Kovancılar	0.020	0.025	0.044	0.158	0.202	0.351	0.252	0.324	0.561
19	Bingöl	0.004	0.005	0.009	0.158	0.202	0.351	0.257	0.330	0.573
20	Karlıova	0.006	0.008	0.014	0.158	0.202	0.351	0.313	0.402	0.696

The comparison of the target displacements for Defne/Hatay, where the highest PGA was measured in the first earthquake, and for the Karlıova/Bingöl provinces, where the lowest PGA was measured, is shown in Figure 11.

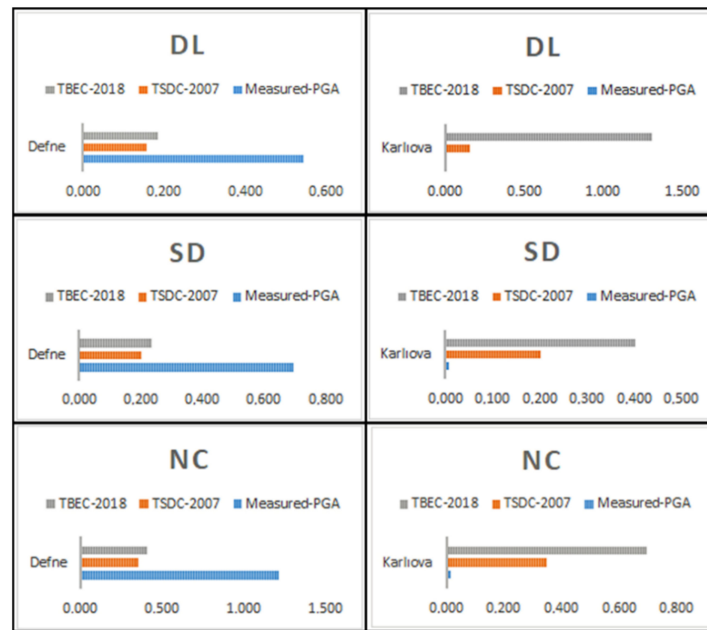


Figure 11. Comparison of the target displacements for Defne and Karliova for first earthquake.

Within the scope of this study, structural analyses were also performed for the second earthquake, the Elbistan earthquake, and target displacements were obtained. The comparison of these values attained by considering the earthquake hazard measured for this earthquake and the last two maps is shown in Table 15.

Table 15. Comparison of measured with predicted limit states for Elbistan earthquake.

No	Location	Limit States (m)								
		Measured PGA			TSDC-2007			TBEC-2018		
		DL	SD	NC	DL	SD	NC	DL	SD	NC
1	Yayladağı	0.004	0.005	0.009	0.158	0.202	0.351	0.147	0.188	0.326
2	Samandağ	0.012	0.016	0.027	0.158	0.202	0.351	0.186	0.238	0.413
3	Defne	0.011	0.014	0.024	0.158	0.202	0.351	0.184	0.236	0.409
4	Hatay	0.013	0.017	0.029	0.158	0.202	0.351	0.177	0.227	0.393
5	Kırıkhan	0.023	0.030	0.052	0.158	0.202	0.351	0.203	0.261	0.452
6	Hassa	0.028	0.035	0.061	0.158	0.202	0.351	0.237	0.305	0.528
7	Islahiye	0.021	0.026	0.046	0.158	0.202	0.351	0.218	0.280	0.486
8	Nurdağı	0.038	0.049	0.084	0.158	0.202	0.351	0.194	0.248	0.431
9	Türkoğlu	0.023	0.030	0.052	0.158	0.202	0.351	0.185	0.237	0.411
10	Pazarcık	0.082	0.106	0.184	0.158	0.202	0.351	0.203	0.261	0.452
11	Gölbaşı	0.051	0.065	0.113	0.158	0.202	0.351	0.201	0.258	0.447
12	Doğanşehir	0.188	0.241	0.417	0.158	0.202	0.351	0.188	0.242	0.419
13	Çelikhan	0.051	0.065	0.113	0.158	0.202	0.351	0.233	0.299	0.519
14	Sincik	0.051	0.065	0.113	0.158	0.202	0.351	0.254	0.325	0.564
15	Pütürge	0.019	0.025	0.043	0.158	0.202	0.351	0.267	0.342	0.593
16	Doğanyol	0.021	0.026	0.046	0.158	0.202	0.351	0.261	0.335	0.581
17	Sivrice	0.028	0.036	0.062	0.158	0.202	0.351	0.254	0.326	0.566
18	Kovancılar	0.028	0.036	0.062	0.158	0.202	0.351	0.252	0.324	0.561
19	Bingöl	0.004	0.005	0.009	0.158	0.202	0.351	0.257	0.330	0.573
20	Karliova	0.004	0.005	0.009	0.158	0.202	0.351	0.313	0.402	0.696

The comparison of the target displacements for Doğanşehir/Malatya, where the highest PGA was measured in the second earthquake, and for Karlıova/Bingöl, where the lowest PGA was measured, is shown in Figure 12.

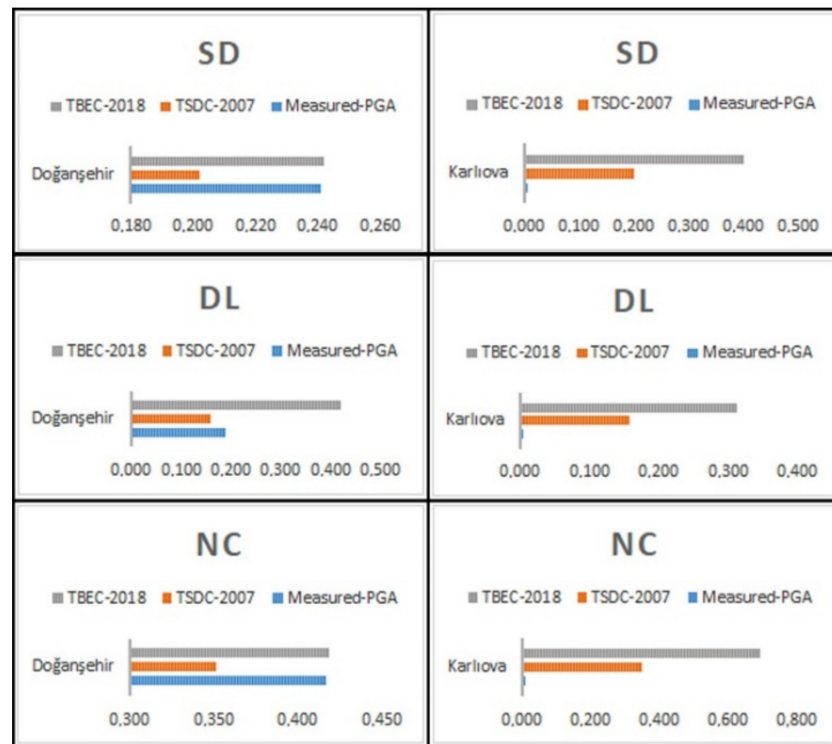


Figure 12. Comparison of the target displacements for Doğanşehir and Karlıova for 2nd earthquake.

The target displacements obtained by considering the measured PGAs in the first earthquake exceeded the displacements obtained for the predicted PGAs in the previous earthquake hazard map for Defne, Hatay, Kırıkhan, Hassa, Islahiye, Nurdağı, and Pazarcık. The largest value was determined in the epicenter of the earthquake, in the Pazarcık (Kahramanmaraş) district. The predicted target displacements in the other settlements other than these settlements provide the displacements obtained for the measured values. In the settlements where the target displacements for the previous earthquake map were exceeded, the displacements predicted in the current earthquake hazard map were also exceeded. There was no exceedance in the remaining settlements. The target displacements obtained by taking into account the measured PGAs for the second earthquake did not exceed the displacements obtained for the predicted PGAs in both earthquake hazard maps. This is an indication that the earthquake hazard is adequately represented in the structural analyses. For the first earthquake, structural analyses were also carried out for the target displacements that exceeded the standard design earthquake ground motion level. The structural analysis was performed again for the ground motion level with a probability of exceedance of 2% in 50 years (recurrence period 2475 years). The comparison of the attained limit state values is shown in Table 16.

Considering the predicted larger earthquake, the limit problem is eliminated for Kırıkhan, Islahiye, and Nurdağı. However, for other settlements, Defne, Hatay, Hassa, and Pazarcık, the target displacements obtained for the measured values for the largest earthquake exceeded the predicted displacements. Examples of exceedances and non-exceeding of these values for the largest earthquake ground motion (DD-1) are shown in Figure 13.

Table 16. Target displacements for DD-1 for earthquakes with larger limit states (m).

Province	Measured PGA			TBEC-2018/DD-1		
	DL	SD	NC	DL	SD	NC
Defne	0.543	0.697	1.208	0.366	0.469	0.813
Hatay	0.474	0.608	1.053	0.346	0.443	0.769
Kırıkhan	0.297	0.381	0.661	0.395	0.507	0.880
Hassa	0.521	0.669	1.159	0.158	0.575	0.997
Islahiye	0.263	0.337	0.585	0.413	0.530	0.919
Nurdağı	0.238	0.306	0.530	0.378	0.485	0.841
Pazarcık	0.876	1.124	1.949	0.370	0.475	0.823

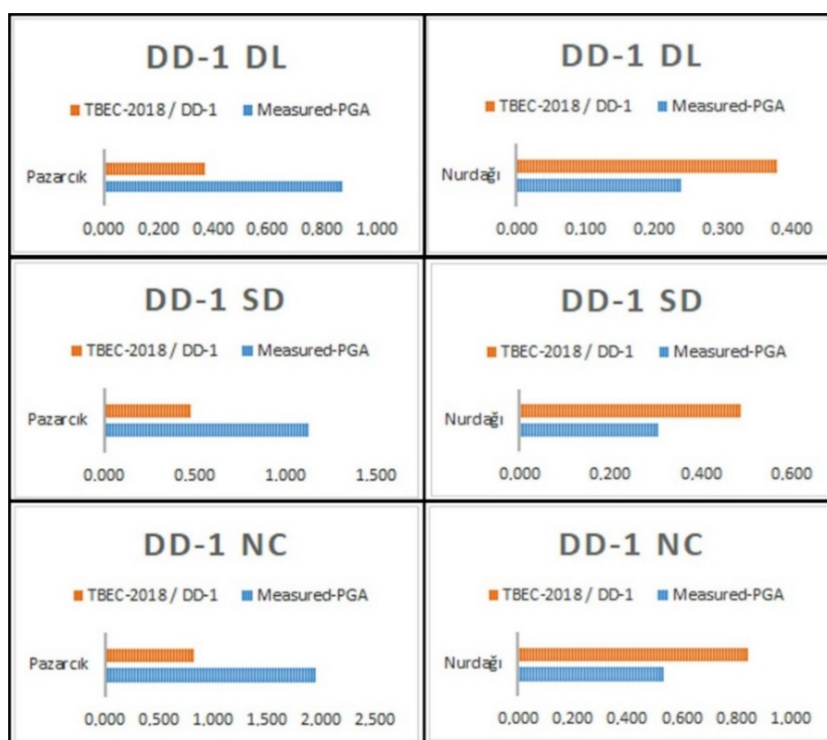


Figure 13. Comparison of target displacement for DD-1.

5. Conclusions

The 6 February 2023 Kahramanmaraş earthquakes, which were the disaster of the century for Türkiye and caused thousands of casualties, clearly revealed Türkiye’s earthquake reality. The fact that the earthquakes happened in succession at two different epicenters on the EAFZ, one of Türkiye’s main tectonic members, further increased the extent of the structural damage. The earthquake pair that occurred on the EAFZ within the instrumental period of earthquake activity caused great destruction in eleven different provinces. The losses caused by the earthquakes have made the EAFZ worth examining. Within the scope of this study, twenty different settlements directly located on this fault zone were taken into consideration. First of all, information about the EAFZ was given. Secondly, the measured and predicted earthquake hazards were compared for the settlements taken into consideration. While the earthquake hazard was sufficiently represented for most settlements, it was not sufficiently represented for the first earthquake in Defne, Hatay, Kırıkhan, Hassa, Islahiye, Nurdağı, or Pazarcık. The values anticipated in the current earthquake hazard map for the second earthquake were not exceeded. At this point, it is necessary to update

the seismic hazard analyses by taking into account these two major earthquakes in order to present the earthquake hazard for these settlements more realistically. Acceleration values give the results that best reflect the ground behavior within the earthquake parameters. Therefore, PGA values also change depending on the differentiation of ground conditions. In the current hazard maps, this situation has been handled more accurately compared to the previous versions and has become changeable depending on the update of the PGA values. Thus, if a new and larger record is obtained at the PGA station, that value is now accepted as the current value. Meanwhile, in places where there are no new records, the values naturally remain lower than the updated values. The predicted PGA, spectral acceleration coefficients, and idealized curve of target displacements in TBEC-2018 should be improved.

The study also investigated the effects of site-specific design spectra used in the design of structures on the target displacements obtained for different settlements on the EAFZ. It is important to note that the site-specific design spectrum curve has a direct and significant impact on displacement requirements. A full correlation was observed between the displacements for damage estimation and the PGA value. As the PGA increases, the expected displacement demands on the structure also rise, indicating that larger ground motions result in greater structural displacements.

As a result of field investigations conducted by the authors in the settlements considered, information was provided about the damage to RC structures. Incomplete, incorrect, or incomplete non-application of earthquake-resistant structural design principles during the project and construction phases increased the extent of the damage. In cases where several of these negativities were used together, the damage levels reached higher levels. In addition to all these, the structures built following earthquake-resistant structural design principles provided life safety performance levels. In addition, the amount of damage increased due to the earthquakes occurring very close to the surface, in the same region, and on the same day, and the aftershocks that occurred afterward. In addition, the effect of local soil conditions was seen, especially in Gölbaşı and Hatay. The exceedance of the structural capacity in the foundations of the structures, liquefaction, and soil amplification effects were observed clearly in Gölbaşı and Hatay. This once again revealed the significance of the earthquake–soil–structure interaction. Different types of irregularities found in RC structures, which are the dominant urban building stock, reduced the earthquake performance of the structures.

In the seismic design codes used in Türkiye, the requirement to use RC shear walls is only valid for basements. It should not be forgotten that the use of RC shear walls will significantly affect the earthquake performance of the structures. In addition to all these, precautions that can be taken before an earthquake are also a part of modern disaster management in terms of reducing earthquake damage. At this point, one of the precautions that can be taken is to make decisions on strengthening or demolishing buildings with inadequate earthquake performance by examining and analyzing the existing building stocks. Using rapid assessment methods in buildings will allow for the determination of risk priorities among the existing building stock.

One of the main causes of structural damage in earthquakes to buildings constructed according to the 2018 regulations is structural irregularities. These irregularities, which reduce the earthquake resistance of the structure, should be avoided and addressed in seismic design codes.

In addition to structural characteristics, which are one of the main causes of earthquake damage, earthquake characteristics and local ground conditions are also effective factors in damage. The correct determination of the standard design ground motion level used in structural analyses depends on the seismic hazard analyses to be performed. It should not be forgotten that the realistic determination of earthquake hazards will affect the earthquake performance of structures due to the target displacements expected from the structures. In this context, the earthquake hazard determined regionally in Türkiye before 2018 has been replaced by site-specific earthquake hazards as of 2018. The earthquake hazard for each

location should be determined at the micro-scale rather than the macro-scale. In settlements where large earthquakes occur, seismic hazard analyses should be taken into account in these earthquakes and the resulting standard design and maximum motion levels should be updated and used.

Within the scope of this study, structural analyses were performed for the sample RC structural model, and target displacements were obtained for the measured and predicted PGAs. The value was below the limit value for the second earthquake. However, the displacement values were exceeded in seven different settlements for the first earthquake. When a larger earthquake predicted for these settlements was taken into account, it was determined that the exceedance continued for Defne, Hatay, Hassa, and Pazarcık. It should not be forgotten that the displacements to be obtained depending on the earthquake hazard will allow for more realistic earthquake performance and loss estimation in structures. The earthquake performance that structures will show in a possible earthquake depends on the realistic presentation of the earthquake hazard.

Finally, to improve the performance of existing RC structures in future earthquakes and to avoid encountering the damage caused by the 6 February 2023 doublet earthquakes, we suggest that future seismic hazard analysis, the design of RC structures, the analysis of target displacements, and predicted limit states are enhanced to take precautions for the next earthquake occurrences. Buildings constructed before 2000 generally require detailed performance evaluations and should be strengthened or demolished and rebuilt according to their risk status.

Author Contributions: Conceptualization, E.I., F.A., A.B., M.H.-N. and H.A.; methodology, E.I., F.A., E.H., A.B. and E.A.; validation, M.H.-N., E.I., A.B., H.A. and E.A.; investigation, E.I., F.A., A.B. and H.A.; resources, M.H.-N., H.A., E.H., A.B. and E.I.; data curation, F.A., E.I., A.B. and H.A.; writing—original draft preparation, F.A., E.I., A.B., H.A. and M.H.-N.; writing—review and editing, E.A., E.H., M.H.-N. and A.B.; visualization, E.A. and F.A.; supervision, E.I., A.B. and F.A.; funding acquisition, M.H.-N., E.H. and E.I. All authors have read and agreed to the published version of the manuscript.

Funding: This research received no external funding.

Data Availability Statement: Data sharing is not applicable.

Acknowledgments: The results presented in this scientific paper have been partially obtained through the research activities within the project 2023-1-HR01-KA220-HED-000165929 “Intelligent Methods for Structures, Elements and Materials” [<https://im4stem.eu/en/home/> (accessed on 25 July 2024)], co-funded by the European Union under the program Erasmus+ KA220-HED—Cooperation partnerships in higher education.

Conflicts of Interest: The authors declare no conflicts of interest.

References

1. Kramer, S.L. Performance-based design methodologies for geotechnical earthquake engineering. *Bull. Earthq. Eng.* **2014**, *12*, 1049–1070. [[CrossRef](#)]
2. Erdik, M.; Fahjan, Y.; Ozel, O.; Alcik, H.; Mert, A.; Gul, M. Istanbul earthquake rapid response and the early warning system. *Bull. Earthq. Eng.* **2003**, *1*, 157–163. [[CrossRef](#)]
3. Inel, M.; Ozmen, H.B.; Bilgin, H. Re-evaluation of building damage during recent earthquakes in Turkey. *Eng. Struct.* **2008**, *30*, 412–427. [[CrossRef](#)]
4. Büyüksaraç, A.; Isik, E.; Harirchian, E. A case study for determination of seismic risk priorities in Van (Eastern Turkey). *Earthq. Struct.* **2021**, *20*, 445–455.
5. Ansal, A.; Kurtuluş, A.; Tönük, G. Seismic microzonation and earthquake damage scenarios for urban areas. *Soil Dyn. Earthq. Eng.* **2010**, *30*, 1319–1328. [[CrossRef](#)]
6. Wang, W.; Li, L.; Qu, Z. Machine learning-based collapse prediction for post-earthquake damaged RC columns under subsequent earthquakes. *Soil Dyn. Earthq. Eng.* **2023**, *172*, 108036. [[CrossRef](#)]
7. Wang, W.; Li, L.; Qu, Z.; Yang, X. Enhanced damage segmentation in RC components using pyramid Haar wavelet downsampling and attention U-net. *Autom. Constr.* **2024**, *168*, 105746. [[CrossRef](#)]

8. Acito, M.; Magrinelli, E.; Milani, G.; Tiberti, S. Seismic vulnerability of masonry buildings: Numerical insight on damage causes for residential buildings by the 2016 central Italy seismic sequence and evaluation of strengthening techniques. *J. Build. Eng.* **2020**, *28*, 101081. [[CrossRef](#)]
9. Milani, G.; Valente, M. Failure analysis of seven masonry churches severely damaged during the 2012 Emilia-Romagna (Italy) earthquake: Non-linear dynamic analyses vs conventional static approaches. *Eng. Fail. Anal.* **2015**, *54*, 13–56. [[CrossRef](#)]
10. Jünemann, R.; de La Llera, J.C.; Hube, M.A.; Cifuentes, L.A.; Kausel, E. A statistical analysis of reinforced concrete wall buildings damaged during the 2010, Chile earthquake. *Eng. Struct.* **2015**, *82*, 168–185. [[CrossRef](#)]
11. Doğangün, A. Performance of reinforced concrete buildings during the May 1, 2003 Bingöl Earthquake in Turkey. *Eng. Struct.* **2004**, *26*, 841–856. [[CrossRef](#)]
12. Manfredi, G.; Prota, A.; Verderame, G.M.; De Luca, F.; Ricci, P. 2012 Emilia earthquake, Italy: Reinforced concrete buildings response. *Bull. Earthq. Eng.* **2014**, *12*, 2275–2298. [[CrossRef](#)]
13. Nemutlu, O.F.; Balun, B.; Sari, A. Damage assessment of buildings after 24 January 2020 Elazığ-Sivrice earthquake. *Earthq. Struct.* **2021**, *20*, 325–335.
14. Decanini, L.D.; De Sortis, A.; Goretti, A.; Liberatore, L.; Mollaioli, F.; Bazzurro, P. Performance of reinforced concrete buildings during the 2002 Molise, Italy, earthquake. *Earthq. Spectra* **2004**, *20*, 221–255. [[CrossRef](#)]
15. Ademović, N.; Toholj, M.; Radonić, D.; Casarin, F.; Komesar, S.; Ugarković, K. Post-earthquake assessment and strengthening of a cultural-heritage residential masonry building after the 2020 Zagreb earthquake. *Buildings* **2022**, *12*, 2024. [[CrossRef](#)]
16. Su, N. Structural evaluations of reinforced concrete buildings damaged by Chi-Chi earthquake in Taiwan. *Pract. Period. Struct. Des. Constr.* **2001**, *6*, 119–128. [[CrossRef](#)]
17. Kam, W.Y.; Pampanin, S.; Elwood, K. Seismic performance of reinforced concrete buildings in the 22 February Christchurch (Lyttleton) earthquake. *Bull. N. Z. Soc. Earthq. Eng.* **2011**, *4*, 239–279.
18. Agarwal, P.; Thakkar, S.K.; Dubey, R.N. Seismic performance of reinforced concrete buildings during Bhuj earthquake of January 26, 2001. *ISET J. Earthq. Technol.* **2002**, *39*, 195–217.
19. Lagomarsino, S. Damage assessment of churches after L'Aquila earthquake (2009). *Bull. Earthq. Eng.* **2012**, *10*, 73–92. [[CrossRef](#)]
20. Adiyanto, M.I.; Majid, T.A.; Nazri, F.M. Nonstructural damages of reinforced concrete buildings due to 2015 Ranau earthquake. *AIP Conf. Proc.* **2017**, *1865*, 090002.
21. Ivanović, S.S.; Trifunac, M.D.; Novikova, E.I.; Gladkov, A.A.; Todorovska, M.I. Ambient vibration tests of a seven-story reinforced concrete building in Van Nuys, California, damaged by the 1994 Northridge earthquake. *Soil Dyn. Earthq. Eng.* **2000**, *19*, 391–411. [[CrossRef](#)]
22. Nagato, K.; Kawase, H. Damage evaluation models of reinforced concrete buildings based on the damage statistics and simulated strong motions during the 1995 Hyogo-ken Nanbu earthquake. *Earthq. Eng. Struct. Dyn.* **2004**, *33*, 755–774. [[CrossRef](#)]
23. Valente, M.; Milani, G. Earthquake-induced damage assessment and partial failure mechanisms of an Italian Medieval castle. *Eng. Fail. Anal.* **2019**, *99*, 292–309. [[CrossRef](#)]
24. Kumar, A.; Hughes, P.N.; Sarhosis, V.; Toll, D.; Wilkinson, S.; Coningham, R.; Acharya, K.P.; Weise, K.; Joshi, A.; Davis, C.; et al. Experimental, numerical and field study investigating a heritage structure collapse after the 2015 Gorkha earthquake. *Nat. Hazards* **2020**, *101*, 231–253. [[CrossRef](#)]
25. Sarhosis, V.; Giarelis, C.; Karakostas, C.; Smyrou, E.; Bal, I.E.; Valkaniotis, S.; Ganas, A. Observations from the March 2021 Thessaly Earthquakes: An earthquake engineering perspective for masonry structures. *Bull. Earthq. Eng.* **2022**, *20*, 5483–5515. [[CrossRef](#)]
26. Qu, Z.; Zhu, B.; Cao, Y.; Fu, H. Rapid report of seismic damage to buildings in the 2022 M 6.8 Luding earthquake, China. *Earthq. Res. Adv.* **2023**, *3*, 100180. [[CrossRef](#)]
27. Naik, S.P.; Rimando, J.M.; Mittal, H.; Rimando, R.E.; Porfido, S.; Kim, Y.S. Reappraisal of the 2012 magnitude (MW) 6.7 Negros Oriental (Philippines) earthquake intensity and ShakeMap generation by using ESI-2007 environmental effects. *Geomat. Nat. Hazards Risk* **2024**, *15*, 2311890. [[CrossRef](#)]
28. Leti, M.; Bilgin, H. Investigation of seismic performance of a premodern RC building typology after November 26, 2019 earthquake. *Struct. Eng. Mech.* **2024**, *89*, 491.
29. Dong, X.; Guo, X.; Luo, R.; Yan, C. Seismic response of multi-story buildings subjected to Luding Earthquake 2022, China considering the deformation saturation theory. *Buildings* **2024**, *14*, 2887. [[CrossRef](#)]
30. Tasiopoulou, P.; Smyrou, E.; Bal, I.E.; Gazetas, G.; Vintzileou, E. *Geotechnical and Structural Field Observations from Christchurch, February 2011 Earthquake, in New Zealand*; Research Report; National Technical University of Athens: Athens, Greece, 2011.
31. Karray, M.; Karakan, E.; Kincal, C.; Chiaradonna, A.; Güli, T.O.; Lanzo, G.; Monaco, P.; Sezer, A. Türkiye Mw 7.7 Pazarçık and Mw 7.6 Elbistan earthquakes of February 6th, 2023: Contribution of valley effects on damage pattern. *Soil Dyn. Earthq. Eng.* **2024**, *181*, 108634. [[CrossRef](#)]
32. Büyüksaraç, A.; Işık, E.; Bektaş, Ö.; Avcil, F. Achieving intensity distributions of 6 February 2023 Kahramanmaraş (Türkiye) earthquakes from peak ground acceleration records. *Sustainability* **2024**, *16*, 599. [[CrossRef](#)]
33. Akar, F.; Işık, E.; Avcil, F.; Büyüksaraç, A.; Arkan, E.; İzol, R. Geotechnical and structural damages caused by the 2023 Kahramanmaraş Earthquakes in Gölbaşı (Adıyaman). *Appl. Sci.* **2024**, *14*, 2165. [[CrossRef](#)]
34. Işık, E.; Avcil, F.; İzol, R.; Büyüksaraç, A.; Bilgin, H.; Harirchian, E.; Arkan, E. Field reconnaissance and earthquake vulnerability of the rc buildings in Adıyaman during 2023 Türkiye earthquakes. *Appl. Sci.* **2024**, *14*, 2860. [[CrossRef](#)]

35. İlhan, O.; İndir, O.; Muratoğlu, G.; İçen, A.; Albayrak, K.; Sandikkaya, M.A.; Askan, A.; Arduino, P.; Taciroğlu, E. Local site effects at the selected stations affected by the February 6 2023 Türkiye earthquake sequences. *Soil Dyn. Earthq. Eng.* **2024**, *178*, 108454. [CrossRef]
36. Ozturk, M.; Arslan, M.H.; Korkmaz, H.H. Effect on rc buildings of 6 February 2023 Turkey earthquake doublets and new doctrines for seismic design. *Eng. Fail. Anal.* **2023**, *153*, 107521. [CrossRef]
37. Altunsu, E.; Güneş, O.; Öztürk, S.; Sorosh, S.; Sarı, A.; Beeson, S.T. Investigating the structural damage in Hatay province after Kahramanmaraş-Türkiye earthquake sequences. *Eng. Fail. Anal.* **2024**, *157*, 107857. [CrossRef]
38. Över, S.; Demirci, A.; Özden, S. Tectonic implications of the February 2023 Earthquakes (Mw7. 7, 7.6 and 6.3) in south-eastern Türkiye. *Tectonophysics* **2023**, *866*, 230058. [CrossRef]
39. Alkan, H.; Büyüksaraç, A.; Bektaş, Ö. Investigation of earthquake sequence and stress transfer in the Eastern Anatolia Fault Zone by Coulomb stress analysis. *Turkish J. Earth Sci.* **2024**, *33*, 56–68. [CrossRef]
40. Yan, K.; Miyajima, M.; Kumsar, H.; Aydan, Ö.; Ulusay, R.; Tao, Z.; Chen, Y.; Wang, F. Preliminary report of field reconnaissance on the 6 February 2023 Kahramanmaraş Earthquakes in Türkiye. *Geoenviron. Disasters* **2024**, *11*, 11. [CrossRef]
41. Atmaca, B.; Ertürk Atmaca, E.; Roudane, B.; Güleş, O.; Demirkaya, E.; Aykanat, B.; Günaydin, M.; Arslan, M.E.; Kahya, V.; Tatar, T.; et al. Field observations and numerical investigations on seismic damage assessment of rc and masonry minarets during the February 6th 2023, Kahramanmaraş (Mw 7.7 Pazarcık and Mw 7.6 Elbistan) earthquakes in Türkiye. *Int. J. Archit. Herit.* **2024**, *1–26*. [CrossRef]
42. Arslan, M.H.; Dere, Y.; Ecemiş, A.S.; Doğan, G.; Özturk, M.; Korkmaz, S.Z. Code-based damage assessment of existing precast industrial buildings following the February 6th, 2023 Kahramanmaraş earthquakes (Pazarcık Mw 7.7 and Elbistan Mw7. 6). *J. Build. Eng.* **2024**, *86*, 108811. [CrossRef]
43. Cetin, K.O.; Soylemez, B.; Guzel, H.; Cakir, E. Soil liquefaction sites following the February 6 2023, Kahramanmaraş-Türkiye earthquake sequence. *Bull. Earthq. Eng.* **2024**, 1–24. Available online: <https://link.springer.com/article/10.1007/s10518-024-01875-3> (accessed on 29 November 2024). [CrossRef]
44. Öser, C.; Sarğın, S.; Yıldırım, A.K.; Korkmaz, G.; Altinok, E.; Kelesoglu, M.K. Geotechnical aspects and site investigations on Kahramanmaraş earthquakes, February 06, 2023. *Nat. Hazards* **2024**. [CrossRef]
45. Sezgin, S.K.; Sakcalı, G.B.; Özen, S.; Yıldırım, E.; Avcı, E.; Bayhan, B.; Çağlar, N. Reconnaissance report on damage caused by the February 6 2023, Kahramanmaraş earthquakes in reinforced-concrete structures. *J. Build. Eng.* **2024**, *89*, 109200. [CrossRef]
46. Binici, B.; Yakut, A.; Kadas, K.; Demirel, O.; Akpınar, U.; Canbolat, A.; Yurtseven, F.; Oztaskin, O.; Aktas, S.; Canbay, E. Performance of RC buildings after Kahramanmaraş Earthquakes: Lessons toward performance based design. *Earthq. Eng. Eng. Vibr.* **2023**, *22*, 883–894. [CrossRef]
47. Cetin, K.O.; Cuceoglu, F.; Ayhan, B.U.; Yildirim, S.; Aydin, S.; Demirdogen, S.; Er, Y.; Gurbuz, A.; Moss, R.E.S. Performance of hydraulic structures during 6 February 2023 Kahramanmaraş, Türkiye, earthquake sequence. *Earthq. Spectra* **2024**, *40*, 2231–2267. [CrossRef]
48. Demir, A.; Celebi, E.; Ozturk, H.; Ozcan, Z.; Ozocak, A.; Bol, E.; Sert, S.; Sahin, F.Z.; Arslan, E.; Yaman, Z.D.; et al. Destructive impact of successive high magnitude earthquakes occurred in Türkiye’s Kahramanmaraş on February 6, 2023. *Bull. Earthq. Eng.* **2024**, 1–27. Available online: <https://link.springer.com/article/10.1007/s10518-024-01865-5> (accessed on 29 November 2024). [CrossRef]
49. Özman, G.Ö.; Selçuk, S.A.; Arslan, A. Image classification on post-earthquake damage assessment: A case of the 2023 Kahramanmaraş earthquake. *Eng. Sci. Technol. Int. J.* **2024**, *56*, 101780. [CrossRef]
50. Yön, B.; Dedeoğlu, İ.Ö.; Yetkin, M.; Erkek, H.; Calayır, Y. Evaluation of the seismic response of reinforced concrete buildings in the light of lessons learned from the February 6, 2023, Kahramanmaraş, Türkiye earthquake sequences. *Nat. Hazards* **2024**, 1–37. Available online: <https://link.springer.com/article/10.1007/s11069-024-06859-9> (accessed on 29 November 2024). [CrossRef]
51. Avcil, F.; Işık, E.; İzol, R.; Büyüksaraç, A.; Arkan, E.; Arslan, M.H.; Aksoylu, C.; Eyisüren, O.; Harirchian, E. Effects of the February 6 2023, Kahramanmaraş earthquake on structures in Kahramanmaraş city. *Nat. Hazards* **2023**, 1–39. Available online: <https://link.springer.com/article/10.1007/s11069-023-06314-1> (accessed on 29 November 2024). [CrossRef]
52. Apostolaki, S.; Riga, E.; Pitolakis, D. Rapid damage assessment effectiveness for the 2023 Kahramanmaraş Türkiye earthquake sequence. *Int. J. Disast. Risk Reduct.* **2024**, *111*, 104691. [CrossRef]
53. Işık, E.; Bilgin, H.; Avcil, F.; İzol, R.; Arkan, E.; Büyüksaraç, A.; Harirchian, E.; Hysenlliu, M. Seismic Performances of Masonry Educational Buildings during the 2023 Türkiye (Kahramanmaraş) Earthquakes. *GeoHazards* **2024**, *5*, 700–731. [CrossRef]
54. Avgın, S.; Köse, M.M.; Özbek, A. Damage assessment of structural and geotechnical damages in Kahramanmaraş during the February 6, 2023 earthquakes. *Eng. Sci. Technol. Int. J.* **2024**, *57*, 101811. [CrossRef]
55. Yuzbasi, J. Post-Earthquake Damage assessment: Field observations and recent developments with recommendations from the Kahramanmaraş earthquakes in Türkiye on February 6th, 2023 (Pazarcık M7. 8 and Elbistan M7. 6). *J. Earthq. Eng.* **2024**, 1–26. [CrossRef]
56. Kırtel, O.; Aydın, F.; Boru, E.; Toplu, E.; Aydın, E.; Sarıbıyık, A.; Dok, G.; Akkaya, A.; Vural, İ.; Öntürk, K.; et al. Seismic damage assessment of under-construction industrial buildings: Insights from the february 2023 Türkiye-Syria earthquakes. *Case Stud. Constr. Mater.* **2024**, *21*, e03507. [CrossRef]
57. Atar, M.; İnce, O.; Taş, Ö.F.; Özmen, A.; Sayın, E. 6 Şubat 2023 Kahramanmaraş depremleri sonrasında betonarme kolonlarda enine donatı kusurlarının incelenmesi. *Firat Üniversitesi Mühendislik Bilim. Derg.* **2024**, *36*, 221–230. [CrossRef]

58. Yetkin, M.; Dedeoğlu, I.Ö.; Gülen, T. February 6 2023, Kahramanmaraş twin earthquakes: Evaluation of ground motions and seismic performance of buildings for Elazığ, southeast of Türkiye. *Soil Dyn. Earthq. Eng.* **2024**, *181*, 108678. [CrossRef]
59. Bol, E.; Özocak, A.; Sert, S.; Çetin, K.Ö.; Arslan, E.; Kocaman, K.; Ayhan, B.U. Evaluation of soil liquefaction in the city of Hatay triggered after the February 6, 2023 Kahramanmaraş-Türkiye earthquake sequence. *Eng. Geol.* **2024**, *339*, 107648. [CrossRef]
60. Şen, F.; Sunca, F.; Altunişik, A.C. Seismic performance assessment of a base-isolated hospital building subjected to February 6, 2023, Kahramanmaraş, Türkiye earthquakes (Mw 7.7 Pazarcık and Mw 7.6 Elbistan) and seismic fragility analysis considering different construction stages. *Soil Dyn. Earthq. Eng.* **2024**, *185*, 108876. [CrossRef]
61. Trifonova, P.; Oynakov, E.; Popova, M.; Aleksandrova, I. Seismic variations before Eastern Anatolian catastrophic events in February 2023. *Nat. Hazards* **2024**, 1–13. Available online: <https://link.springer.com/article/10.1007/s11069-024-06831-7> (accessed on 29 November 2024). [CrossRef]
62. Balun, B. Developing a regression model for predicting the seismic input energy of rc buildings using 6 February 2023 Kahramanmaraş Earthquake. *Türk Doğa Fen Derg.* **2024**, *13*, 142–151. [CrossRef]
63. Zuo, H.; Bi, K.; Hao, H.; Ma, R. Influences of ground motion parameters and structural damping on the optimum design of inerter-based tuned mass dampers. *Eng. Struct.* **2021**, *227*, 111422. [CrossRef]
64. Felicetta, C.; Mascandola, C.; Spallarossa, D.; Pacor, F.; Hailemichael, S.; Di Giulio, G. Quantification of site effects in the Amatrice area (Central Italy): Insights from ground-motion recordings of the 2016–2017 seismic sequence. *Soil Dyn. Earthq. Eng.* **2021**, *142*, 106565. [CrossRef]
65. Kamal, M.; İnel, M. Correlation between Ground motion parameters and displacement demands of mid-rise rc buildings on soft soils. *Buildings* **2021**, *12*, 125. [CrossRef]
66. Akkar, S.; Sandikkaya, M.A.; Bommer, J.J. Empirical ground-motion models for point-and extended-source crustal earthquake scenarios in Europe and the Middle East. *Bull. Earthq. Eng.* **2014**, *12*, 359–387. [CrossRef]
67. Delavaud, E.; Cotton, F.; Akkar, S.; Scherbaum, F.; Danciu, L.; Beauval, C.; Drouet, S.; Douglas, J.; Basili, R.; Sandikkaya, M.A.; et al. Toward a ground-motion logic tree for probabilistic seismic hazard assessment in Europe. *J. Seismol.* **2012**, *16*, 451–473. [CrossRef]
68. Bommer, J.J.; Stafford, P.J.; Alarcón, J.E.; Akkar, S. The influence of magnitude range on empirical ground-motion prediction. *Bull. Seismol. Soc. Am.* **2007**, *97*, 2152–2170. [CrossRef]
69. Bulajić, B.Đ.; Pavić, G.; Hadzima-Nyarko, M. PGA vertical estimates for deep soils and deep geological sediments—A case study of Osijek (Croatia). *Comput. Geosci.* **2022**, *158*, 104985. [CrossRef]
70. Kale, Ö.; Akkar, S.; Ansari, A.; Hamzehloo, H. A ground-motion predictive model for Iran and Turkey for horizontal PGA, PGV, and 5% damped response spectrum: Investigation of possible regional effects. *Bull. Seismol. Soc. Am.* **2015**, *105*, 963–980. [CrossRef]
71. Sandikkaya, M.A.; Akkar, S.; Bard, P.Y. A nonlinear site-amplification model for the next pan-European ground-motion prediction equations. *Bull. Seismol. Soc. Am.* **2013**, *103*, 19–32. [CrossRef]
72. Işık, E.; Ekinci, Y.L.; Sayil, N.L.; Büyüksaraç, A.; Aydin, M.C. Time-dependent model for earthquake occurrence and effects of design spectra on structural performance: A case study from the North Anatolian Fault Zone, Turkey. *Turk. J. Earth Sci.* **2021**, *30*, 215–234. [CrossRef]
73. Liu, J.; Wang, W.; Dasgupta, G. Pushover analysis of underground structures: Method and application. *Sci. China Technol. Sci.* **2014**, *57*, 423–437. [CrossRef]
74. Elnashai, A.S. Advanced inelastic static (pushover) analysis for earthquake applications. *Struct. Eng. Mech.* **2001**, *12*, 51–69. [CrossRef]
75. Shendkar, M.R.; Kontoni, D.P.N.; Işık, E.; Mandal, S.; Maiti, P.R.; Harirchian, E. Influence of masonry infill on seismic design factors of reinforced-concrete buildings. *Shock. Vib.* **2022**, *2022*, 5521162. [CrossRef]
76. Chopra, A.K.; Goel, R.K. A modal pushover analysis procedure for estimating seismic demands for buildings. *Earthq. Eng. Struct. Dyn.* **2002**, *31*, 561–582. [CrossRef]
77. Krawinkler, H.; Seneviratna, G.D.P.K. Pros and cons of a pushover analysis of seismic performance evaluation. *Eng. Struct.* **1998**, *20*, 452–464. [CrossRef]
78. Kim, S.; D’Amore, E. Push-over analysis procedure in earthquake engineering. *Earthq. Spectra.* **1999**, *15*, 417–434. [CrossRef]
79. Deierlein, G.G. Overview of comprehensive framework for earthquake performance assessment. In Proceedings of the International Workshop of Performance—Based Seismic Design Concept and Implementation, Bled, Slovenia, 28 June–1 July 2004; pp. 15–26.
80. Habibi, A.; Jami, E. Correlation between ground motion parameters and target displacement of steel structures. *Int. J. Civil. Eng.* **2017**, *15*, 163–174. [CrossRef]
81. Xue, Q.; Chen, C.C. Performance-based seismic design of structures: A direct displacement-based approach. *Eng. Struct.* **2003**, *25*, 1803–1813. [CrossRef]
82. Fajfar, P. Capacity spectrum method based on inelastic demand spectra. *Earthq. Eng. Struct. Dyn.* **1999**, *28*, 979–993. [CrossRef]
83. Aydinoglu, M.N. A response spectrum-based nonlinear assessment tool for practice: Incremental response spectrum analysis (IRSA). *ISST J. Earthq. Technol.* **2007**, *44*, 169–192.
84. Kutanis, M.; Boru, O.E. The need for upgrading the seismic performance objectives. *Earthq. Struct.* **2014**, *7*, 401–414. [CrossRef]

85. Alpyürür, M.; Ulutaş, H. Comparison of performance analysis results with developed site-specific response spectra and Turkish seismic design code: A case study from the SW Türkiye region. *Buildings* **2024**, *14*, 1233. [CrossRef]
86. Güneş, N.; Ulucan, Z.Ç.; Erdoğan, A.S. Yakın fay yer hareketlerinin yön etkisi. *Niğde Ömer Halisdemir Üniversitesi Mühendislik Bilim. Derg.* **2013**, *2*, 21–33. [CrossRef]
87. Güneş, N. Yakın Fay yer Hareketleri ve Performansa Dayalı Tasarıma Uyarlanmaları. Ph.D. Thesis, Fırat Üniversitesi, Fen Bilimleri Enstitüsü, Elâzığ, Türkiye, 2009.
88. Işık, E.; Harirchian, E. A comparative probabilistic seismic hazard analysis for Eastern Turkey (Bitlis) based on updated hazard map and its effect on regular RC structures. *Buildings* **2022**, *12*, 1573. [CrossRef]
89. Işık, E.; Hadzima-Nyarko, M.; Bilgin, H.; Ademović, N.; Büyüksaraç, A.; Harirchian, E.; Bulajić, B.; Özmen, H.B.; Aghakouchaki Hosseini, S.E. A comparative study of the effects of earthquakes in different countries on target displacement in mid-rise regular rc structures. *Appl. Sci.* **2022**, *12*, 12495. [CrossRef]
90. Isık, E. Comparative investigation of seismic and structural parameters of earthquakes ($M \geq 6$) after 1900 in Turkey. *Arab. J. Geosci.* **2022**, *15*, 971. [CrossRef]
91. Bilgin, H.; Hadzima-Nyarko, M.; Işık, E.; Ozmen, H.B.; Harirchian, E. A comparative study on the seismic provisions of different codes for RC buildings. *Struct. Eng. Mech.* **2022**, *83*, 195–206.
92. Işık, E.; Harirchian, E.; Büyüksaraç, A.; Ekinçi, Y. L Seismic and structural analyses of the eastern anatolian region (Turkey) using different probabilities of exceedance. *Appl. Syst. Innov.* **2021**, *4*, 89. [CrossRef]
93. Yılmaz, H.; Over, S.; Ozden, S. Kinematics of the east Anatolian Fault zone between turkoglu (Kahramanmaraş) and celikhan (adiyaman), eastern Turkey. *Earth Planets Space* **2006**, *58*, 1463–1473. [CrossRef]
94. Nalbant, S.S.; McCloskey, J.; Steacy, S.; Barka, A.A. Stress accumulation and increased seismic risk in eastern Turkey. *Earth Planet. Sci. Lett.* **2002**, *195*, 291–298. [CrossRef]
95. Utkucu, M.; Budakoğlu, E.; Çabuk, M. Teleseismic finite-fault inversion of two $M_w = 6.4$ earthquakes along the East Anatolian Fault Zone in Turkey: The 1998 Adana and 2003 Bingöl earthquakes. *Arab. J. Geosci.* **2018**, *11*, 1–14. [CrossRef]
96. Ambraseys, N.N. Some characteristic features of the Anatolian fault zone. *Tectonophysics* **1970**, *9*, 143–165. [CrossRef]
97. Arpat, E.; Şaroğlu, F. Doğu Anadolu Fayı ile ilgili bazı gözlemler ve düşünceler. *Bull. Miner. Res. Expl.* **1972**, *78*, 44–50.
98. Şaroğlu, F.; Emre, O.; Kuscu, I. The East Anatolian fault zone of Turkey. *Ann. Tectonicae* **1992**, 99–125.
99. Tatar, O.; Piper, J.D.A.; Gürsoy, H.; Heimann, A.; Koçbulut, F. Neotectonic deformation in the transition zone between the Dead Sea Transform and the East Anatolian Fault Zone, Southern Turkey: A palaeomagnetic study of the Karasu Rift Volcanism. *Tectonophysics* **2004**, *385*, 17–43. [CrossRef]
100. Aksoy, E.; Inceoz, M.; Koçyiğit, A. Lake Hazar basin: A negative flower structure on the east anatolian fault system (EAFS), SE Turkey. *Turk. J. Earth Sci.* **2007**, *16*, 319–338.
101. Büyüksaraç, A.; Bektaş, Ö.; Alkan, H. Fault modeling around southern Anatolia using the aftershock sequence of the Kahramanmaraş earthquakes ($M_w = 7.7$ and $M_w = 7.6$) and an interpretation of potential field data. *Acta Geophys.* **2024**, *72*, 2985–2996. [CrossRef]
102. Bayrak, E.; Ozer, C. The 24 January 2020 ($M_w 6.8$) Sivrice (Elazığ, Turkey) earthquake: A first look at spatiotemporal distribution and triggering of aftershocks. *Arab. J. Geosci.* **2021**, *14*, 2445. [CrossRef]
103. AFAD. Available online: <https://depem.afad.gov.tr/event-historical> (accessed on 20 July 2024).
104. Calvi, V.S. Erdbebenkatalog der Turkei und Einiger Benaehbarter Gebiete. *MTA Rep.* **1941**, 276.
105. Sbeinati, M.R.; Darawcheh, R.; Mouty, M. The historical earthquakes of Syria: An analysis of large and moderate earthquakes from 1365 BC to 1900 AD. *Ann. Geophys.* **2005**. Available online: <https://www.earth-prints.org/server/api/core/bitstreams/3fff4914-a300-4d98-b08d-8233437b071c/content> (accessed on 29 November 2024). [CrossRef]
106. Köküm, M.; Özçelik, F. An example study on re-evaluation of historical earthquakes: 1789 Palu (Elazığ) earthquake, Eastern Anatolia, Turkey. *Bull. Miner. Res. Expl.* **2020**, *161*, 157–170.
107. Sunkar, M. *Major Earthquakes and Their Effects on Settlements in Palu (Elazığ) in the Historical and Instrumental Period*; International Palu Symposium Proceedings 2018; Harput Applied and Research Center Fırat University: Elazığ, Türkiye, 2018.
108. KOERI. Historical Earthquakes. Available online: <https://www.koeri.boun.edu.tr> (accessed on 22 July 2024).
109. AFAD. 24 Ocak 2020 Sivrice (Elazığ) $M_w 6.8$ Depremi Raporu, Ankara. Erişim Adresi. 2020. Available online: <https://depem.afad.gov.tr/depemdokumanlari/1831> (accessed on 22 July 2024).
110. Bayik, C.; Gurbuz, G.; Abdikan, S.; Gormus, K.S.; Kutoglu, S.H. Investigation of source parameters of the 2020 Elazığ-Sivrice Earthquake ($M_w 6.8$) in the East Anatolian Fault Zone. *Pure Appl. Geophys.* **2022**, *179*, 587–598. [CrossRef]
111. Dogan, G.; Ecemis, A.S.; Korkmaz, S.Z.; Arslan, M.H.; Korkmaz, H.H. Buildings damages after Elazığ, Turkey earthquake on January 24, 2020. *Nat. Hazards* **2021**, *109*, 161–200. [CrossRef]
112. Çağlar, N.; Vural, I.; Kirtel, O.; Saribiyik, A.; Sumer, Y. (Structural damages observed in buildings after the January 24, 2020 Elazığ-Sivrice earthquake in Türkiye. *Case Stud. Constr. Mater.* **2023**, *18*, e01886. [CrossRef]
113. Taymaz, T.; Ganas, A.; Yolsal-Çevikbilen, S.; Vera, F.; Eken, T.; Erman, C.; Keleş, D.; Kapetanidis, V.; Valkaniotis, S.; Karasante, I.; et al. Source mechanism and rupture process of the 24 January 2020 $M_w 6.7$ Doğanyol–Sivrice earthquake obtained from seismological waveform analysis and space geodetic observations on the East Anatolian Fault Zone (Turkey). *Tectonophysics* **2021**, *804*, 228745. [CrossRef]

114. Alkan, H.; Büyüksaraç, A.; Bektaş, Ö.; Işık, E. Coulomb stress change before and after 24.01. 2020 Sivrice (Elazığ) earthquake (Mw= 6.8) on the East Anatolian Fault Zone. *Arab. J. Geosci.* **2021**, *14*, 2648. [CrossRef]
115. Barbot, S.; Luo, H.; Wang, T.; Hamiel, Y.; Piatibratova, O.; Javed, M.T.; Braitenberg, C.; Gurbuz, G. Slip distribution of the February 6, 2023 Mw 7.8 and Mw 7.6, Kahramanmaraş, Turkey earthquake sequence in the East Anatolian fault zone. *Seismica* **2023**, *2*, 10417588. [CrossRef]
116. Zhang, Y.; Tang, X.; Liu, D.; Taymaz, T.; Eken, T.; Guo, R.; Zheng, Y.; Wang, J.; Sun, H. Geometric controls on cascading rupture of the 2023 Kahramanmaraş earthquake doublet. *Nat. Geosci.* **2023**, *16*, 1054–1060. [CrossRef]
117. Palo, M.; Zollo, A. Small-scale segmented fault rupture along the East Anatolian fault during the 2023 Kahramanmaraş earthquake. *Commun. Earth Environ.* **2024**, *5*, 431. [CrossRef]
118. Tan, O. Long-term aftershock properties of the catastrophic 6 February 2023 Kahramanmaraş (Türkiye) earthquake sequence. *Acta Geophys.* **2024**. Available online: <https://link.springer.com/article/10.1007/s11600-024-01419-y> (accessed on 29 November 2024). [CrossRef]
119. AFAD. *06 Şubat 2023 Pazarcık-Elbistan (Kahramanmaraş) Mw: 7.7—Mw: 7.6 Depremleri Raporu*; Deprem ve Risk Azaltma Genel Müdürlüğü Deprem Dairesi Başkanlığı: Geneva, Switzerland, 2023.
120. Vuran, E.; Serhatoğlu, C.; Timurağaoğlu, M.; Smyrou, E.; Bal, I.E.; Livaoglu, R. Damage observations of RC buildings from 2023 Kahramanmaraş earthquake sequence and discussion on the seismic code regulations. *Bull. Earthq. Eng.* **2024**, 1–30. Available online: <https://link.springer.com/article/10.1007/s10518-023-01843-3> (accessed on 29 November 2024). [CrossRef]
121. Wang, B.; Barbot, S. Rupture segmentation on the East Anatolian fault (Turkey) controlled by along-strike variations in long-term slip rates in a structurally complex fault system. *Geology* **2024**, *52*, 779–783. [CrossRef]
122. AFAD. 2024. Available online: <https://deprem.afad.gov.tr/home-page> (accessed on 25 July 2024).
123. Emre, Ö.; Duman, T.Y.; Özalp, S.; Şaroğlu, F.; Olgun, Ş.; Elmacı, H.; Çan, T. Active fault database of Turkey. *Bull. Earthq. Eng.* **2018**, *16*, 3229–3275. [CrossRef]
124. Türkiye Cumhuriyeti Cumhurbaşkanlığı. Available online: <https://www.sbb.gov.tr/wp-content/uploads/2023/03/2023-Kahramanmaraş-ve-Hatay-Depremleri-Raporu.pdf> (accessed on 10 November 2024).
125. TBEC. *Turkish Building Earthquake Code*; T.C. Resmi Gazete: Ankara, Türkiye, 2018.
126. AFAD. 2024. Available online: <https://tdth.afad.gov.tr> (accessed on 15 June 2024).
127. AFAD-TADAS. Disaster and Emergency Management Presidency Department of Earthquake Turkish Accelerometric Database and Analysis System. 2023. Available online: <https://tadas.afad.gov.tr/> (accessed on 15 December 2023).
128. Seismosoft. SeismoStruct 2024—A Computer Program for Static and Dynamic Nonlinear Analysis of Framed Structures. 2024. Available online: <http://www.seismosoft.com> (accessed on 10 February 2024).
129. EN 1998-3; Eurocode-8: Design of Structures for Earthquake Resistance-Part 3: Assessment and Retrofitting of Buildings. European Committee for Standardization: Brussels, Belgium, 2005.
130. Antoniou, S.; Pinho, R. Seismostruct—Seismic Analysis Program by Seismosoft. In *Technical Manual and User Manual*; Seismosoft: Pavia, Italy, 2022.
131. Celep, Z. Betonarme sistemlerde doğrusal olmayan davranış: Plastik mafsallı kabulü ve çözümleme. In *Altıncı Ulusal Deprem Mühendisliği Konferansı*; Chamber of Civil Engineers: İstanbul, Türkiye, 2007; pp. 16–20.
132. Sümer, Y. Determining plastic hinge length of high performance RC beams. *Acad. Platf.-J. Eng. Sci.* **2016**, *5*, 39–47.
133. Alıcıoğlu, M.B. Çelik kiriş ve kolon plastik mafsallı parametrelerinin ve şekil değiştirme sınır değerlerinin karşılaştırmalı incelenmesi. *ALKÜ Fen Bilim. Derg.* **2021**, *3*, 25–41. [CrossRef]
134. Pinto, P.E.; Franchin, P. Eurocode 8-Part 3: Assessment and retrofitting of buildings. In *Proceedings of the Eurocode 8 Background and Applications, Dissemination of Information for Training*, Lisbon, Portugal, 10–11 February 2011.

Disclaimer/Publisher's Note: The statements, opinions and data contained in all publications are solely those of the individual author(s) and contributor(s) and not of MDPI and/or the editor(s). MDPI and/or the editor(s) disclaim responsibility for any injury to people or property resulting from any ideas, methods, instructions or products referred to in the content.